ATPase activity of KaiC is a key determinant of the circadian oscillation of cyanobacterial KaiABC clock

Dissertation for the fulfillment of the doctoral degree

DAS Sumita
Department of Computational Science and Engineering
Graduate School of Engineering
Nagoya University
2018

Abstract

Circadian clock is a biological machinery inducing a rhythm of approximately 24 hours, which pertains to all kingdoms of life and helps to organize the behavior of organisms with the day-night cycle. In the test tube, the circadian rhythm of cyanobacterial Kai proteins can be reconstituted when three Kai proteins, KaiA, KaiB and KaiC, are incubated in the presence of ATP; the phosphorylation level of KaiC exhibits a robust circadian oscillation. KaiC forms a hexamer complex and shows ATPase activity; each subunit of KaiC hexamer hydrolyzes about 15 ATP molecules/day. This ATPase activity is very low compared to the other ATPase enzymes and plays an important role in defining the circadian period. In particular, the frequency of the phosphorylation cycle of KaiC is closely correlated to the ATPase activity of KaiC. Furthermore, the ATPase activity of the truncated CI domain of KaiC shows correlation to the circadian frequency in the CII domain. All these observations suggest that ATPase activity in the CI domain plays a central role to generate the circadian period of the Kai oscillator. However, how the ATP hydrolysis in the CI domain drives the oscillation remains elusive. Here, we quantitatively investigate the role of ATP hydrolysis of KaiABC clockwork using mathematical modeling. We thereby propose two coarse-grained theoretical models, the many-molecule model (MM) and the single-molecule model (SM) to understand the macroscopic synchronization of a large number of KaiC molecules and the microscopic reactions and structural transition in individual KaiC molecules; these two models were developed to unify macroscopic and microscopic viewpoints of KaiC system. Our models are based on the assumptions that conformational transition of KaiC hexamer takes place between two structural states and that the binding interactions among Kai proteins, phosphorylation/dephosphorylation reactions, and ATP hydrolysis depend on this

transition. We also assume that the structural transition is induced by these reactions; therefore, multifold feedback relations are constituted among reactions and structural transition in the proposed models. Results of these two theoretical models give insights to elucidate the role of ATP hydrolysis. In the simulation results with these models, ATP hydrolysis in the CI domain of KaiC hexamer is a driving mechanism of the oscillation of individual KaiC hexamers, which brings oscillation in the ensemble-level molecules and the ATP hydrolysis is necessary for synchronizing oscillations of a large number of KaiC hexamers. Sensitive temperature dependence of the lifetime of the ADP bound state in the CI domain makes the oscillation period temperature insensitive. ATPase activity is correlated to the frequency of phosphorylation oscillation in a single molecule of KaiC hexamer, which should be the origin of the observed ensemble-level correlation between the ATPase activity and the frequency of phosphorylation oscillation. Thus, the simulation results with the MM and SM models suggest that ATP hydrolysis stochastically occurring in each CI domain of individual KaiC hexamers is a key process for oscillatory behaviors of the ensemble of many KaiC hexamers.

List of Contents Page

Chapter 1: Introduction

One of the fundamental survival properties of the organisms is their ability to adapt to the rapidly changing environments. Most biological systems can respond to the stress conditions, such as temperature and/or pH changes and starvation, in a highly effective manner. However, organisms cannot take the precautions for such environmental changes in advance as they appear to happen randomly. On the contrary to these random events, the daily and annual rhythms are determined by the planetary movement of the earth in the solar system. The rotation of the earth generates a rhythm of light and temperature on its surface, which can be predicted in advance. Almost all life on the planet earth, including human, employs an internal biological timer to anticipate these daily changes in light, temperature and so on. Thus, it is anticipated that the biological timer evolved since the early phase of the evolutionary history of life. The possession of such biological clock allows organisms to optimize their physiology and behavior in advance of the varied demand of the day/night cycle. The internally generated daily rhythms are known as the 'circadian rhythm'. The term 'circadian' originated from the two Latin words *circa* (about) and *dies* (day). Therefore, the circadian phenomenon stands for biological activities with a frequency of one activity cycle for approximately every 24-hour (Halberg et al., 1977).

1.1 Concepts of circadian rhythm

The rhythmic nature of daily activity can be described by three terms that correspond to the characteristic description of a waveform: period, phase and amplitude, which are illustrated in Figure1.

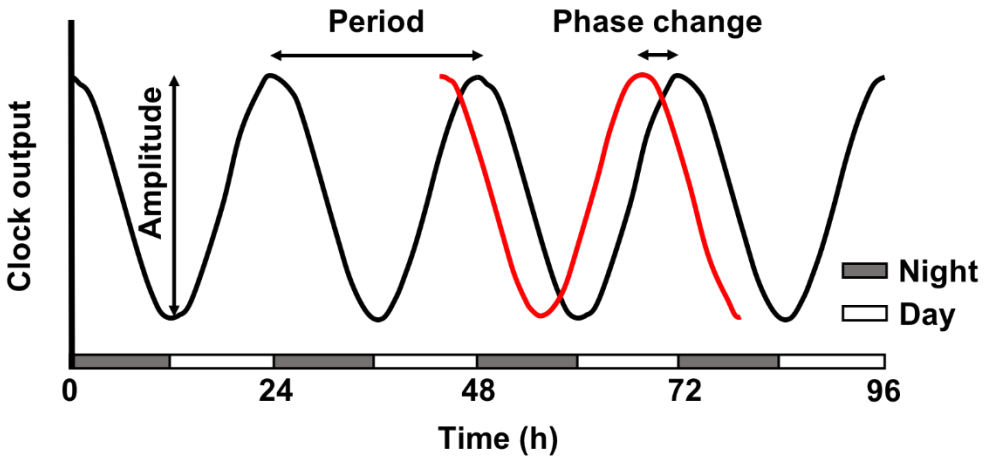

Figure 1: Properties of a circadian rhythm. The solid black line indicates a circadian oscillation. Every cycle sustains for around 24-hours. Characteristics of a circadian rhythm, including period, amplitude and phase changes are denoted by arrows. The red line shows phase advance in this example.

In a typical circadian rhythm, the level of a measured quantity varies with the day-night cycle (Figure 1). The point at the highest level of an oscillation is known as the peak and the point at the lowest level is called the trough. These points, the peak and the trough, can be used to state the internal activity according to the environmental cues. The difference between peak and trough in the measured level is the amplitude of the rhythm. The phase of a circadian rhythm is the timing of a reference point in the cycle (for example, the peak or trough) relative to the fixed event (for example, light or dark onset) (DeCoursey et al., 2004). The timing of any given point in the day can be represented by its phase. The time interval between the two reference points with identical

phases, for example, two peaks or two troughs, is called the period of the rhythm. The phase shift can be either a phase advance or phase delay compared with a control example.

The internal clock must fulfil the following three characteristics which define the existence of a biological clock. The first intrinsic characteristic of the clock is a free-running period of approximately 24-hours under constant environmental conditions, for example under constant temperature, and either constant light or constant darkness. Accordingly, the circadian oscillator must be endogenous, meaning that the oscillation can take place in the absence of external cues. Second, the circadian oscillation must be entrainable to the external cues, e.g. light or temperature. Therefore, the circadian system can adapt to the changes in the environment. When the organism is subjected to the natural light-dark condition, the circadian clock must respond to the local environmental cues. The third defining feature of the circadian clock is that the period must remain almost unchanged upon temperature variation within the physiological range. This essential feature of the biological clock is known as 'temperature compensation'.

A basic model of a circadian rhythm consists of three fundamental elements that are shown in Figure 2. First, the environmental cues (zeitgebers), which convey external information including the time of day and temperature to a central oscillator. Second, the oscillator, also known as the pacemaker, which is responsible for maintaining and disseminating the 24-hour time information. It is entrainable by the external zeitgebers. The environmental cues are received and internalized by the circadian oscillator, which will then translate them into the alterations in the activity of genes or proteins. Finally, the outputs pathway, which relays the temporal information of the central oscillator into the whole organism to maintain the circadian oscillation (Figure 2).

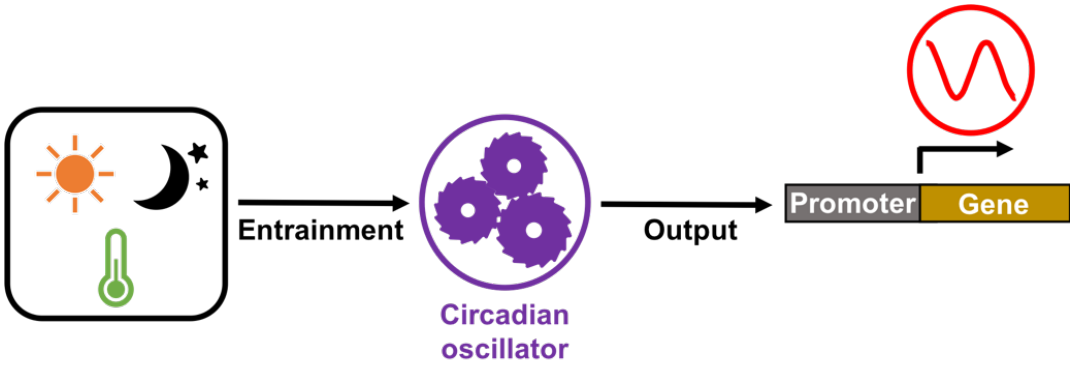

Figure 2: A basic model of a biological clock that consists of three basic elements: environmental entrainments, a central oscillator, and an output pathway. The circadian oscillator integrates the environmental cues and results in gene-expression regulation, which conveys the oscillatory message to the whole organism.

1.2 Historical outlooks

The concept of an internal rhythm was described in 1729 by a French astronomer Jean-Jacques d'Ortous de Mairan for the first time, who found that the leaves of heliotrope plants were continuously opening and closing even in the constant darkness (DD) (de Mairan 1729). His work initiated a new field of biology called chronobiology, which describes the interaction between the circadian clock and the physiology of an organism. In the modern field of chronobiology, the circadian clock of human has been systematically studied in the bunker experiments lead by Jürgen Aschoff (Aschoff, 1967, 1969; Aschoff & Wever, 1976). In the absence of any external zeitgebers, the volunteers, living inside the bunker for several weeks, displayed various free-running rhythms. This study has shown that human displays a slightly longer period (~25h) of endogenous rhythm on average. The experiments further revealed that without external stimuli the sleep-wake rhythms

become dissociated from the temperature cycles. In this seminal study, Aschoff concluded that human possesses a weakly connected multi-oscillatory system, which is composed of virtually as many clocks as the number of cells.

However, the first evidence for a genetic basis of circadian activity was brought to light by the independent groups working on fruit flies and fungus. The circadian rhythms of insects have been first described by Konopka on *Drosophila pseudoobscura* and *Drosophila melanogaster*. The first clock gene identified was named *period* (*per*) (Konopka & Benzer, 1971). Many prokaryotes undergo cellular division even for multiple times within a single day. Thus, it was believed that an endogenous pacemaker with an approximate 24-hour period did not seem to be useful for prokaryotes. Therefore, it was assumed that circadian rhythms exist only in eukaryotes. However, many strains of cyanobacteria (chlorophyll-containing prokaryotic bacteria) are capable of autotrophic photosynthesis as well as nitrogen fixation. Interestingly, it was found that even under constant light condition light-light (LL)**,** the rhythmic nitrogen fixation ability, as measured by the activity of nitrogenase enzyme, showed its peak phase in the subjective night of the cyanobacterium *Oscillatoria* sp. (Stal & Krumbein, 1985). Apparently, the facts of photosynthesis and nitrogenase activity of cyanobacteria seem to be contradictory to each other since photosynthesis peaked during the subjective daytime while nitrogen fixation was active during the subjective night. However, one year later, another study was reported claiming that the rhythmic nitrogen fixation activity was temporally separated from photosynthesis as a way to reconcile these two contradictory processes (Mitsui et al., 1986). Meanwhile, Huang and colleagues were apparently the first to recognize that cyanobacteria clearly exhibit circadian rhythms of nitrogen fixation activity. In their study, they demonstrated the significant characteristics of circadian rhythms in the unicellular freshwater cyanobacterium, *Synechococcus* sp. RF-1 (Huang &

Grobbelaar, 1995; Grobbelaar et al., 1986). This ground-breaking observation has motivated many scientists to further study the circadian clocks in cyanobacteria. Eventually, cyanobacteria have become a model organism for analyzing the molecular components of biological clocks inside the cell. This was partly because of the fact that prokaryotes show much simpler interaction which helps researchers to avoid much more complex interactions among multiple oscillators in eukaryotes. Moreover, studying the cyanobacteria helps us to know the evolution of circadian clocks, as they are one of the oldest organisms on earth known to possess an internal clock.

Later on, Kondo and colleagues have established *Synechococcus elongatus* (*S. elongatus*) PCC 7942 as a model organism for circadian rhythms in prokaryotes. In an influential study, Kondo et al., have shown that the promoter activity of a specific reporter strain exhibits circadian behavior (Kondo et al., 1993). The authors introduced a set of bacterial reporter genes into the cyanobacterial construct. This construct contained a set of luciferase gene called *luxAB* from the *Vibrio harveyi* under control of cyanobacterial promoter *psbAI* (a *Synechococcus* photosystem II gene) introduced into the neutral site I on the chromosome. The activity of the luciferase gene, that is bioluminescence, was measured and it was found that cyanobacteria show circadian rhythm in luciferase activity similar to that found in eukaryotes and this can satisfy all three criteria of circadian rhythms: Firstly, the rhythm persists in the light-light (LL) after one light-dark (LD) cycle entrainment with a period of ~24-hours (endogenous). Secondly, after being entrained previously to LD cycles that were 12-hours out of phase, the time course of bioluminescence in LL showed robust opposite-phase-traces (entrainable). Finally, the bioluminescence exhibited similar free-running periods under three different constant temperatures: 25, 30 and 36°C, leading to a calculated Q_{10} of 1.1 (temperature compensated) where Q_{10} is a factor by which the reaction rate is accelerated with the temperature increase of 10°C. Moreover, the rhythm was abolished by

adding either a photosystem II inhibitor or an inhibitor of bacterial translation, suggesting that the rhythm originates from the cyanobacteria, not from any contaminant eukaryotes (Kondo et al., 1993).

A mutation analysis in cyanobacterium *Synechococcus elongatus* strain PCC 7942 further demonstrated that this circadian rhythm originates from the complex interactions between a clock gene cluster called *kaiABC,* which consists of three genes, *kaiA*, *kaiB* and *kaiC*, and their corresponding Kai proteins, KaiA, KaiB and KaiC (Ishiura et al., 1998). Hereafter in this thesis, we use the common abbreviations where *kaiB* and *kaiC* are collectively denoted as *kaiBC*, and likewise, KaiA, KaiB and KaiC are denoted as KaiABC, etc. Using mutational mapping and bioluminescence assay analysis, Ishiura et al. reported that the circadian rhythm of gene expression in this cyanobacterium is controlled by three genes, *kaiA*, *kaiB* and *kaiC*. Moreover, it was shown that the protein products of the clock gene *kaiC* negatively regulate their own gene expression, which generates an auto-regulatory feedback loop. This feedback loop can cause the clock genes to oscillate in a circadian manner. Remarkably, not only the mRNA transcription of *kaiA* and *kaiBC*, but also the abundance of KaiB and KaiC proteins were found to be rhythmic in *S. elongatus.* Overexpression of the *kaiA* gene causes an enhancement of *kaiBC* gene transcription, while overexpression of *kaiC* represses it. Thus, the negative feedback control by KaiC, which generates a circadian oscillation in *kaiC* expression, is sustained by KaiA through enhancing the *kaiC* expression. (Ishiura et al., 1998). The fact that the clock genes are under negative regulation by one of their protein products and positive regulation by another does fit the transcriptional and translational feedback loop (TTFL) model (Dunlap, 1999).

However, the auto-regulatory TTFL model was strongly criticized by a study on cyanobacterial cells in constant darkness. In early 2005, Tomita and colleagues reported that the

phosphorylation of KaiC protein occurs in a circadian manner in the constant darkness which also shows temperature compensation and persists even in the presence of a transcription or translation inhibitor (Tomita et al., 2005). In this study, authors examined the accumulation profiles of *kaiA* mRNA and *kaiBC* mRNA either under DD or LL condition. Although the expression of *kaiBC* mRNA showed robust circadian rhythms in the LL, when cells were transferred to the DD conditions from the light, the *kaiBC* mRNA was reduced to almost undetectable level within 4 hours, suggesting that the *de novo* expression of clock genes was abolished in the constant darkness which is in contradiction to the TTFL model. On the contrary, in accumulation profiling of KaiABC at the protein expression level was found to be constant at the DD, suggesting their stability in the darkness. More remarkably, KaiC protein is phosphorylated and dephosphorylated, and the phosphorylation level of KaiC showed robust circadian rhythm in the DD that lasted even up to 56 hours, which was comparable to what was found in LL. The KaiC phosphorylation rhythm continued under a condition in which neither the transcription of *kaiBC* nor the translation of the protein products was permitted. The results clearly suggested the existence of a circadian rhythm in the post-translational modification level of KaiC where neither the transcription nor the translation is necessary (Tomita et al., 2005), which showed discrepancies of the picture based on the TTFL mechanism.

1.3 The *in vitro* KaiABC system

Discrepancies of the TTFL mechanism were resolved when another influential study was published a few months later in 2005, where the circadian oscillator was successfully reconstituted in a test tube by incubating three Kai proteins, KaiA, KaiB and KaiC, along with ATP (Nakajima et al., 2005) (Figure 3). In this experiment, the reaction mixture contained neither mRNA nor DNA

and the amount of protein molecules remained constant, which indicated that protein-protein interactions and the associated hydrolysis of ATP are sufficient to generate the rhythm in the absence of transcriptional or translational processes. We call this *in vitro* system the KaiABC system.

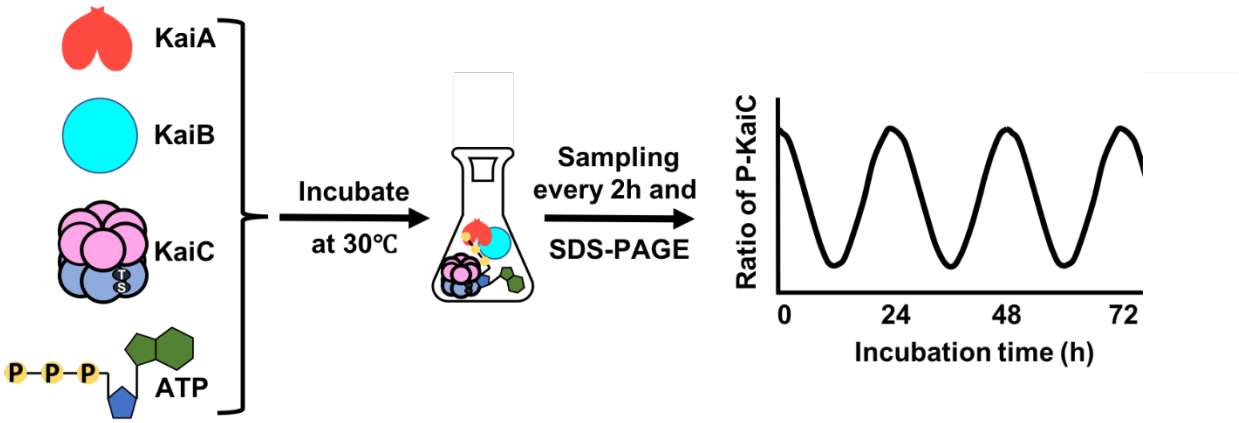

Figure 3: *In vitro* reconstitution of the phosphorylation rhythm of KaiC protein. Three different Kai proteins, KaiA, KaiB and KaiC, were purified, extracted and mixed with ATP molecules *in vitro* at the temperature of 30°C. Samples were collected every 2-hours and were subjected to sodium dodecyl sulfate-polyacrylamide gel electrophoresis (SDS-PAGE) experiments. This experiment can separate and quantify phosphorylated and unphosphorylated KaiC molecules. The ratio of phosphorylated KaiC to the total amount of KaiC was plotted (Nakajima et al., 2005).

Most surprisingly, the period of this *in vitro* protein oscillation was found to be temperature compensated, as in *in vivo* clocks (Nakajima et al., 2005; Tomita et al., 2005). The length of the period of the *in vitro* oscillation of KaiC phosphorylation was found to be 22, 21, and 20 hours at 25, 30, and 35°C, respectively. This leads to a calculated value of Q_{10} to 1.1, which is near the

value observed in the *in vivo* gene expression system (Kondo et al., 1993). These findings have suggested that the post-translational oscillator (PTO) might function as the core clock machinery in cyanobacteria. In the following studies, the *in vitro* interactions between Kai proteins were characterized with great detail. KaiC protein has both the autophosphatase and autokinase activities, and it was found that the binding of KaiA enhances autophosphorylation of KaiC (Iwasaki et al., 2002; Nishiwaki et al., 2004)**,** whereas KaiB attenuates the activity of KaiA to promote auto-dephosphorylation of KaiC (Kitayama et al., 2003; Xu et al.,2003a).

1.4 Structure of Kai proteins and their complexes

It was previously impossible to perform detailed quantitative biophysical, biochemical, and structural analyses of the molecular nature of a circadian clockwork because of the complexity in *in vivo* system and unavailability of an *in vitro* system. Thus, the *in vitro* reconstitution of the circadian oscillation of the KaiABC system made a start of wide-ranging studies in different disciplines and sub-disciplines. Moreover, the structure and function of the three clock proteins have also been studied extensively. To date, the cyanobacterial clock remains the only system in which all essential proteins of the core oscillator have been crystallized and structurally determined. This consequence is important because structural information enables the analyses truly at the molecular level. Now, we can interpret the effect of mutations on the structure-function of the clock proteins, and we can also make precise predictions in which clock proteins interact and influence each other's activity.

The structure of cyanobacterial KaiA was studied by several groups and solved by solution nuclear magnetic resonance (NMR) (Vakonakis & LiWang, 2004) and X-ray crystallography

(Garces et al., 2004; Ye et al., 2004). The KaiA from *S. elongatus* is a 65.3 kDa homodimer (Figure 4).

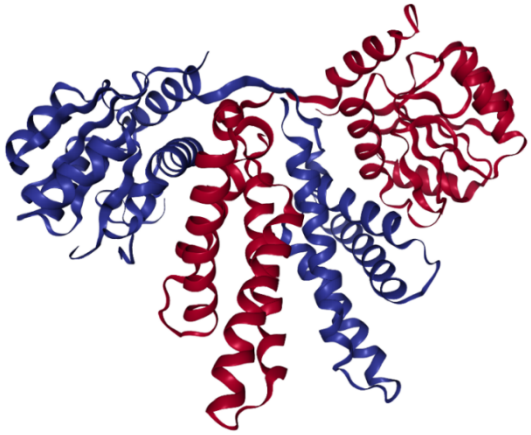

Figure 4: A ribbon style representation of the crystal structure of KaiA dimer from *Synechococcus elongatus* strain PCC 7942 (Image from the RCSB PDB http://www.rcsb.org/). Two different subunits that form the homodimer are colored differently for representations. X-ray diffraction method was used to resolve the structure with the resolution of 2.03 Å. The structure was adapted from PDB (PDB code: 1R8J) which was deposited by Ye. et al., (Ye et al., 2004) .

The structure of KaiA protein is composed of N-terminal and C-terminal domains (Ye et al., 2004). The N-terminal domain of KaiA acts as a module that senses environmental changes in the redox state and then modulates the KaiC phosphorylation cycle (Wood et al., 2010). On the other hand, the C-terminal domain of KaiA is responsible for its dimerization and forms a concave surface (Uzumaki et al., 2004) to recruit the C-terminal region of KaiC (Akiyama et al., 2008; Pattanayek et al., 2006; Vakonakis & LiWang, 2004).

KaiB from *S. elongatus* is composed of 102 amino acid residues and its molecular weight is 11.4 kDa. It is the smallest among the three Kai proteins. The crystal structure of cyanobacterial KaiB revealed an α-β meander motif (Garces et al., 2004; Hitomi et al., 2005). In the absence of both KaiA and KaiC, KaiB from *S. elongatus* (Akiyama et al., 2008), *Synechocystis* PCC6803 (Hitomi et al., 2005), and *Thermosynechococcus elongatus* (Iwase et al., 2005) were observed to remain homo-tetramers (45.6 kDa) in solution by small-angle X-ray scattering (SAXS), dynamic light scattering, and analytical ultracentrifuge (AUC) techniques (Figure 5).

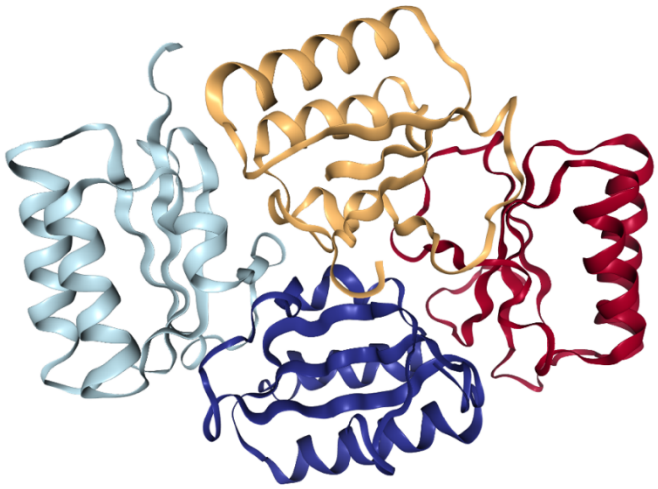

Figure 5: A ribbon style representation of the crystal structure of KaiB homo-tetramer from *Synechocystis sp.* (strain PCC 6803 / Kazusa) (Image from the RCSB PDB https://www.rcsb.org/). Four different subunits that form the homo-tetramer were colored differently for representations. X-ray diffraction method was used to resolve the structure with the resolution of 1.9 Å. The structure was adapted from PDB (PDB code: 1WWJ) which was deposited by Hitomi and colleagues (Hitomi et al., 2005).

KaiC is the largest Kai protein; *S. elongatus* KaiC has 519 amino acid residues (58.0 kDa). Egli and colleagues have reported the detailed crystal structure of the core protein *S. elongatus* KaiC at 2.8 Å resolution (Pattanayek et al., 2004) (Figure. 6). This crystal structure revealed that KaiC is a homo-hexameric ring shape protein composed of six identical protomers. Each protomer of KaiC consists of tandemly duplicated N-terminal (CI) and C-terminal (CII) domains and a C-terminal tail part (Figure. 6). All six protomers are assembled into a double-doughnut-shape with six CI/CII domains comprising CI/CII ring. An ATP molecule incorporated into every CI–CI and CII–CII interface, which counts for a total of 12 ATPs (Pattanayek et al., 2004). It was reported that the presence of ATP stimulates the formation of the hexamer (Mori et al., 2002). KaiC has two phosphorylation sites in the CII domain, Ser431 and Thr432. Both the residues are repeatedly phosphorylated and then dephosphorylated in the following manner: $KaiC^{S/pT} \rightarrow KaiC^{pS/pT} \rightarrow KaiC^{pS/T} \rightarrow KaiC^{S/T}$, where 'S' and 'T' represent Ser431 and Thr432 respectively, 'pS' represents phosphorylated Ser431 and 'pT' represents phosphorylated Thr432 (Nishiwaki et al., 2004; Rust et al., 2007; Xu et al., 2004). The C-terminal tail (residues 498–519), which is important for KaiA binding (Vakonakis et al., 2004), is adjacent to a hairpin loop structure called the A-loop (residues 488–497) (Pattanayek et al., 2004) (Figure 6). KaiC mutants that lack the A-loop and C-terminal tail are of particular interest because they remain phosphorylated even without KaiA (Kim et al., 2008)**,** suggesting the importance of the A-loop in balancing autokinase and autophosphatase activity in KaiC.

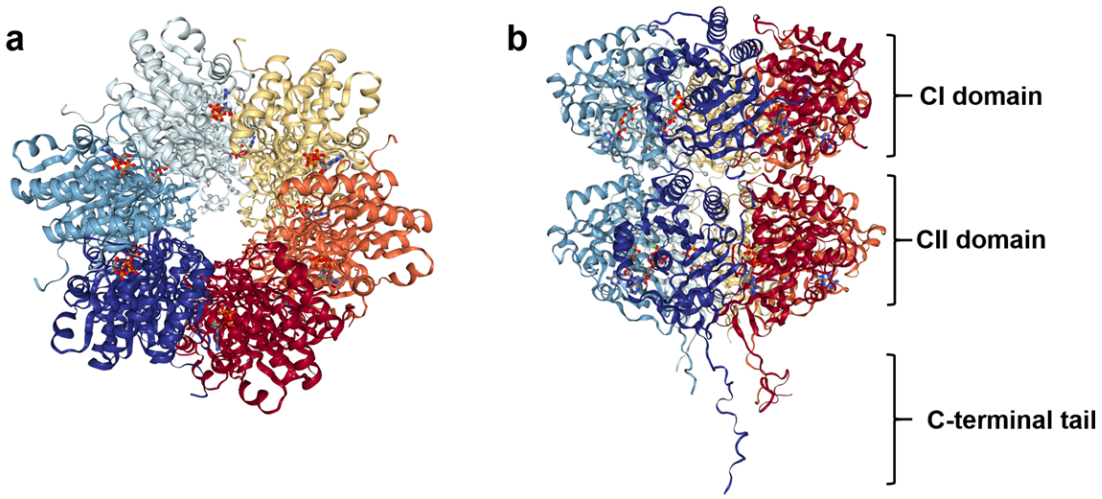

Figure 6: Crystal structure of full-length circadian clock protein KaiC hexamer. Figure shows the ribbon style representations of KaiC forming a hexamer from *Synechococcus elongatus* (strain PCC 7942) (Image from the RCSB PDB https://www.rcsb.org/). Top (**a**) and side (**b**) views. CI and CII domains and the C-terminal tails are marked in the side view. Individual subunits were colored differently for representations. X-ray diffraction method was used to resolve the structure with the resolution of 2.8 Å. The positions of ATPs are shown by ball and stick model in red color. The structure was adapted from PDB (PDB code: 3DVL) which was deposited by Pattanayek, and Egli (*unpublished*).

Although the structure of individual Kai proteins was studied extensively, the core mechanism underlying the circadian periodicity would remain unanswered unless the interaction scheme of Kai protein complexes was resolved. A robust circadian rhythm requires interactions among the Kai proteins. Dynamic complex formation of Kai proteins was first investigated by Kageyama and colleagues both *in vivo* (Kageyama et al., 2003) and *in vitro* (Kageyama et al.,

2006) using size-exclusion chromatography and pull-down analyses. The authors observed that the amount of the complex of KaiA, KaiB and KaiC (KaiABC complex) reaches a maximum level during the middle of the dephosphorylation phase. A small percentage of the KaiC molecules bind to KaiA throughout the cycle, whereas KaiB binds to KaiC preferentially during the dephosphorylation phase. Interestingly, the abilities of the KaiC mutants to bind KaiA increased in the presence of KaiB, suggesting that the KaiC-KaiB complex increases the affinity of KaiC for KaiA (Nishiwaki et al., 2007).

The interaction schemes can be inferred by resolving the structure of Kai protein complexes. Based on the site-directed mutagenesis studies and negatively stained electron microscopy (EM) images of the complex from *S. elongatus* and *T. elongatus* KaiAC, Pattanayek et al. suggested two different models for KaiA binding to the KaiC hexamer (Pattanayek et al., 2006). One is called the 'tethered' model, in which KaiA dimer binds to the tip of the elongated C-terminal tail that is approximately 35 Å away from the CII ring. According to this 'tethered' model of KaiAC interaction, the KaiA dimer becomes tethered to the barrel of hexameric KaiC via a flexible linker region (Figure 7A). This flexible binding increases the probability that a second more transient interaction between KaiA and KaiC might occur between additional surfaces. Another model of KaiAC interaction, which the authors named as the 'engaged' model, also fits the EM density as the tethered model. According to this model, KaiA is in close proximity and binds directly to the CII domain of the hexameric barrel (Figure 7B). A closer interaction between KaiA and KaiC was suggested for the *S. elongatus* KaiAC complex by small-angle X-ray scattering (SAXS) (Akiyama et al., 2008). In this model, KaiA is located near the bottom of the CII ring, thereby establishing an interaction via an association interface ranging from the CII domain to the C-terminal tail. Although it seems essential to characterize the Kai complexes along

a reaction coordinate, the KaiA-KaiC binding model shows similarity in different individually performed studies.

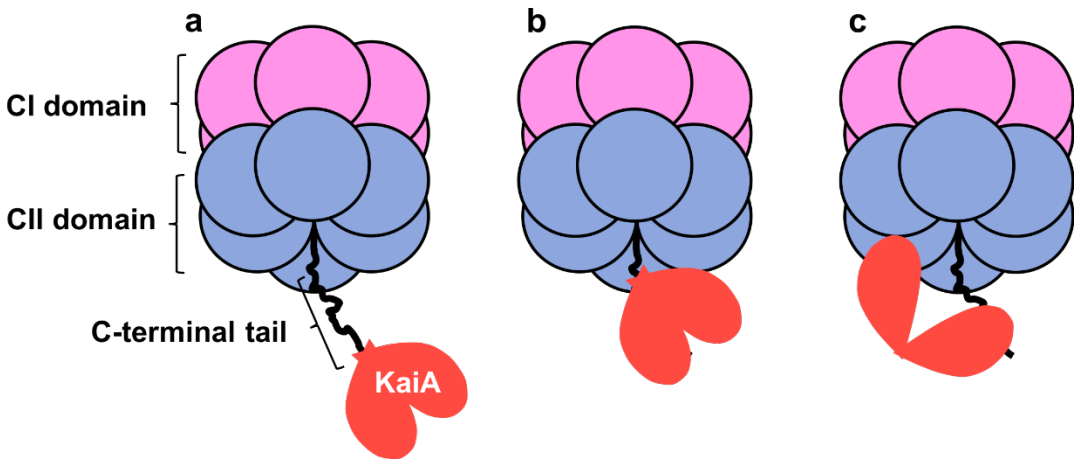

Figure 7: Models of the KaiA-KaiC interaction. Tethered (**a**), engaged (**b**) and SAXS (**c**) models. **a**) According to the 'tethered' model of the KaiAC interaction, a KaiA dimer binds to the tip of the elongated C-terminal tail approximately 35 Å away from the CII ring (Pattanayek et al., 2006). **b**) Similar representation of the 'engaged' model as in the tethered model in panel **a**. According to the engaged model of the KaiAC interaction, KaiA binds directly to the CII domain of the hexameric barrel of KaiC (Pattanayek et al., 2006). **c**) According to the SAXS model, a much broader and closer interaction is achieved between KaiA and KaiC (Akiyama et al., 2008).

It is now widely accepted that the KaiA dimer binds to the C-terminal tails of KaiC hexamer. Thus, we also assumed in our models that KaiA binds to the CII ring of KaiC as a dimer. Although a KaiA dimer, which is denoted here by A_2, binds to the C-terminal tail of the CII domain according

to all three models explained so far, we do not know which model explains the KaiAC interaction in the best possible way. However, if the interaction between A_2 and a particular CII domain is strong, the reaction rates in a specific CII domain becomes different from others and the reaction rates should become heterogeneous in a hexamer. Because there is no experimental report showing that a particular subunit has different reaction rates from the other five subunits, the interaction between A_2 and the body of the CII should be either weak or dynamically fluctuate, which allows the equal opportunity for the interaction of A_2 to all six subunits on average. Therefore, in this dissertation, we do not assume that A_2 binds to a particular CII domain, and rather we assume that A_2 binds to the CII ring and that six CII domains in the ring are equally perturbed by the A_2 binding.

On the other hand, the binding affinity between KaiB and KaiC was first examined by surface plasmon resonance (SPR) analysis by Kageyama and colleagues (Kageyama et al., 2006). This study showed that high levels of KaiC phosphorylation induce the association of KaiB with the KaiC hexamer, which inactivates KaiA to begin the dephosphorylation phase. In contrast, KaiB becomes dissociated from KaiC by reducing KaiC phosphorylation and reactivating KaiA. Moreover, two structural models, the SAXS model and the EM model, were proposed, in which a major constituent of the KaiBC complex possesses a molecular mass of ~400 kDa (Akiyama et al., 2008). These two models exhibited the same molecular mass and binding of KaiB to the CII ring, but they differed in the oligomeric state of the bound KaiB. In the SAXS model, KaiB binds as a homotetramer onto the KaiC hexamer, and in the EM model, two KaiB dimers bind to the CII side of the KaiC hexameric barrel.

More recently, Snijder and colleagues performed an extensive study to analyze the native assemblies of protein complexes by mass spectrometry (MS) and monitored numerous co-occurring Kai protein assembly stoichiometries (Snijder et al., 2017). By freezing the clock in a

single stoichiometry, the authors determined the structure by hydrogen–deuterium exchange, cross-linking mass spectrometry and cryo-EM, and showed that six KaiB molecules bind cooperatively to the CI domains to form a complex of KaiC hexamer and six KaiB molecules, C_6B_6 , which further binds to six KaiA dimers and forms $C_6B_6A_{12}$ (Figure 8).

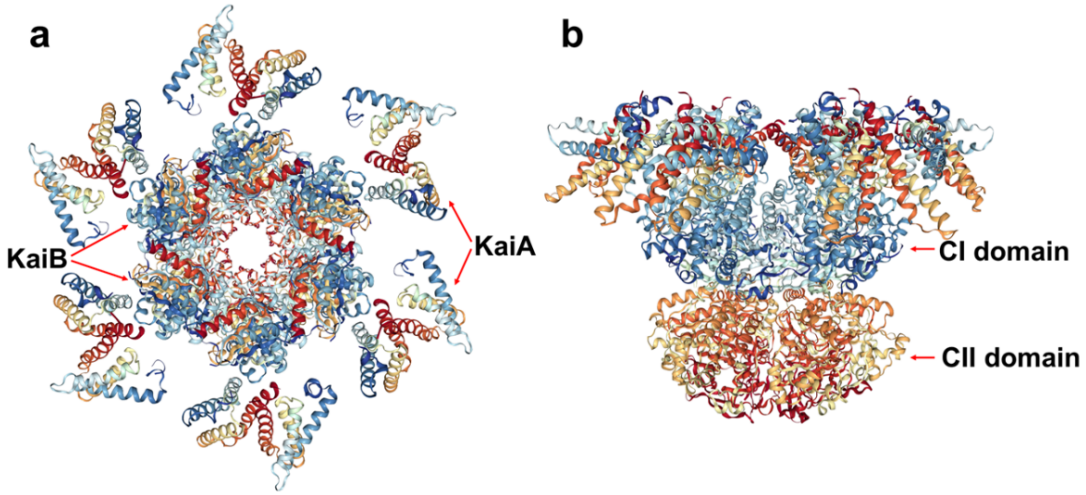

Figure 8: The structure model of KaiABC complex reconstituted from a cryo-EM density. The top view (**a**) and the side view (**b**) of the backbone structure model of KaiABC complex from *S. elongatus* (strain PCC 7942). In each subunit, chains are colored from blue (N-terminal) to red (C-terminal). EM method and single particle reconstruction method were used to resolve the structure with the resolution of 4.7 Å. Fluctuating C-terminal tails were not resolved in this structure model. The structure was adapted from PDB (PDB code: 5N8Y) which was deposited by Snijder and colleagues (Snijder et al., 2017).

This study provides a most reliable model of KaiB-KaiC binding to date. This is partly because of the fact that the cryo-EM method provides detailed atomic structural information and thus shows more direct observation than SAXS. Therefore, in the present study, we propose our mathematical models based on the finding by Snijder and colleagues. Furthermore, based on the MS observation, they described the coexistence of complexes of $C_6B_6A_{2j}$ with $0 \leq j \leq 6$ in a solution (Snijder et al., 2017). Therefore, it is reasonable to assume that A_2 dynamically binds and dissociates to/from C_6B_6 to show the saturation as in the $C_6B_6A_{12}$ complex. In the present model, we use the cryo-EM and the MS observations as bases of our modeling and we further generalize the kinetic scheme to allow the dynamical binding and dissociation of B to/from C_6 by considering $C_6B_iA_{2j}$ with $i \leq j \leq 6$.

1.5 Contribution of ATPase activity of KaiC to circadian pacemaking

The free energy source that drives the Kai oscillator is ATP as the ATP hydrolysis by KaiC appears to be the only step that supplies free energy to the whole events of the KaiABC system. However, precise quantification of ATP consumption during the reaction revealed several outstanding properties of the ATPase activity of KaiC (Terauchi et al., 2007). The rate of ATP hydrolysis of KaiC has been found to be extremely slow, which is around 15 molecules/day/KaiC subunit. This value is far lower than other ATPase enzymes, for example, a myosin molecule, which functions as the molecular motor to generate the force required in muscles; myosin consumes one ATP molecule in every second or sub-second. Moreover, this exceptionally slow ATPase activity of KaiC shows the circadian modulation *in vitro,* in the presence of KaiA and KaiB. A KaiC mutant that has only the CI domain was found to lack the phosphorylation sites and exhibits approximately 70% of the ATPase activity of the full-length KaiC (Terauchi et al., 2007). A similar observation was also reported for *T. elongatus* KaiC, which further confirmed the fact

that the CII domain exhibits intrinsically lower ATPase activity than the CI domain (Murakami et al., 2008). Both CI and CII domains can bind and hydrolyze ATP, but the role of ATP hydrolysis in the CII domain should be tightly related to the phosphorylation reactions in the CII domain. Recent experiments have revealed that the phosphorylation and dephosphorylation of the CII domain proceed via the transfer of phosphate groups between the threonine/serine residues and the nucleotide bound to the CII domain (Egli et al., 2012; Nishiwaki & Kondo, 2012), which suggested that the ATPase activity in the CII domain is necessary for phosphorylation. Therefore, we can expect that several ATP molecules hydrolyzed in each CII domain per one day may be used to phosphorylate two specific sites in each CII domain per one day with the approximate efficiency of about 50%.

More importantly, the most outstanding feature of this ATPase activity is the strong correlation between ATPase activity and the circadian frequency of the phosphorylation rhythm of KaiC. This correlation was observed by measuring the ATPase activity of KaiC without either KaiA or KaiB. This ATPase activity was linearly correlated to the frequency of the phosphorylation cycle measured in the presence of both KaiA and KaiB (Terauchi et al., 2007). Furthermore, the ATPase activity of the truncated CI in the non-oscillatory condition shows correlation to the oscillation frequency of the phosphorylation level in the CII domain in the oscillatory condition (Abe et al., 2015). In addition, the ATPase activity of KaiC also shows strong temperature compensation even in the non-oscillatory condition (Terauchi et al., 2007). These observations suggested that the dynamical state change of the CI induced by the ATPase activity in the CI is a pacemaker of the KaiC oscillation, but the mechanism how the ATP hydrolysis in the CI affects the phosphorylation/dephosphorylation in the CII remains unclear. Therefore,

theoretical study is necessary for elucidating the mechanism, and the present work is the first attempt to resolve this problem.

The ATPase activity is dominated by the CI ring, whereas the phosphorylation/dephosphorylation reactions take place on the CII ring; therefore, the interplay between the ATPase reactions and the phosphorylation/dephosphorylation reactions should be mediated by a coordinated structural coupling between the CI and CII domains. Relations between reactions and structure transition were emphasized by the SAXS (Murayama et al., 2011), the NMR spectroscopy (Chang et al., 2011; Chang et al., 2012), and the biochemical analysis (Oyama et al., 2016). These observations showed that KaiC hexamer during the phase of phosphorylation takes a different structure from that during the phase of dephosphorylation. Moreover, the ATPase activity was reported to be interlocked with the dynamic motions of KaiC (Murayama et al., 2011). Therefore, theoretical models that explain the ATPase reactions should suitably describe the coupling between ATPase reactions and structure transition in KaiC.

1.6 Models of the KaiABC system

In order to elucidate the mechanism of KaiABC core oscillator, we need to understand both the microscopic atomic-scale dynamics of reactions in individual molecules and the macroscopic ensemble-level synchronization among many KaiC molecules; because the ensemble-level oscillation vanishes when individual molecules oscillate independently of each other, synchronization of a macroscopically large number of molecules is necessary for maintaining the coherent oscillation as observed in test tube. Thus, it is important to understand mechanisms at both microscopic and macroscopic levels. The ATPase activity in the CI is regulated by the microscopic structural state of individual molecules, and at the same time,

seriously affects the macroscopic ensemble-level oscillation. Therefore, analyses of the role of ATPase activity in the CI should provide an important clue for understanding the relation between microscopic mechanism to generate the oscillation and the macroscopic mechanism of synchronization.

Many theoretical models were developed previously by describing the concentrations of various molecular species with continuous variables in kinetic differential equations to model the ensemble-level macroscopic dynamics of the oscillating system (Hatakeyama & Kaneko, 2012; Iwasaki et al., 2002; Nagai et al., 2010; Phong et al., 2013; Takigawa-Imamura & Mochizuki, 2006; van Zon et al., 2007; Wang et al., 2009). In these theoretical studies, KaiA sequestration was proposed as a possible mechanism of synchronization of oscillations of many KaiC molecules. Takigawa-Imamura and Mochizuki (Takigawa-Imamura & Mochizuki, 2006) and van Zon et al. (van Zon et al., 2007) suggested that when KaiA binds to a particular state of the KaiC hexamer, the binding depletes the concentration of free unbound KaiA. When the total concentration of KaiA is not large, this depletion of free unbound KaiA reduces the probability of binding of KaiA to the other state which promotes phosphorylation of KaiC. Therefore, consumption (i.e., sequestration) of KaiA by a particular state of a KaiC hexamer reduces the phosphorylation rate of the other KaiC hexamer, which gives rise to the indirect interaction among KaiC hexamers and possibly leads to the synchronized oscillations. This hypothesis of the KaiA sequestration mechanism, which was derived from theoretical modeling, was later supported experimentally by the finding that the oscillation vanishes when the KaiA concentration is larger than a certain threshold (Nakajima et al., 2010). However, there remained arguments on which state KaiA is sequestered to. Takigawa-Imamura and Mochizuki (Takigawa-Imamura & Mochizuki, 2006), van Zon et al. (van Zon et al., 2007), and Hatakeyama and Kaneko (Hatakeyama & Kaneko, 2012)

assumed that KaiA is sequestrated to the unphosphorylated KaiC, while Rust et al. (Rust et al., 2007) assumed that KaiA is sequestrated to the highly phosphorylated KaiC. On the other hand, Brettschneider et al. (Brettschneider et al., 2010), Phong et al. (Phong et al., 2013), and Paijmans et al. (Paijmans et al., 2017) assumed that KaiA is sequestered to the KaiABC complex. The recent combined analyses of EM structural observation and mass spectrometry of the KaiABC complex (Snijder et al., 2017) showed that maximally six dimers of KaiA can bind to a KaiBC complex, which should give a significant effect of sequestration of KaiA, and thereby supported the hypothesis of the KaiA sequestration to the KaiABC complex. In the present thesis, we develop theoretical models by assuming the KaiA sequestration to the KaiABC complex and assuming the stoichiometry found by Snijder et al (Snijder et al., 2017) in the KaiABC complex.

Other models described the system with the Monte Carlo methods by explicitly considering stochastic phosphorylation/dephosphorylation reactions in individual molecules and stochastic binding reactions among many molecules (Eguchi et al., 2008; Mori et al., 2007; Nagai et al., 2010; van Zon et al., 2007; Yoda et al., 2007). These Monte Carlo-type models should be useful for analyzing the relation between microscopic and macroscopic mechanisms. However, the ATP hydrolysis reactions and the activated intramolecular dynamics with ATP consumption were not considered in these models. Though experimental observations have revealed the importance of the ATPase activity of KaiC in the oscillation of the Kai system (Terauchi et al., 2007, Abe et al., 2015), the mechanism of how the ATPase activity influences the oscillation has not been analyzed much in theoretical studies. Roles of ATPase activity was first intensively discussed theoretically by Paijmans et al. (Paijmans et al., 2017) by using a Monte Carlo-type model of KaiC molecules. As suggested in the model of Paijmans et al., ATP molecules bound in the CII should be used for phosphorylating Ser431 and Thr432 through the ATPase activity in the CII. However, the role of

ATPase reactions in the CI remained unresolved. Paijmans et al. argued that the ATPase activity in the CI helps synchronization of many KaiC molecules and that it does not play a role in generating oscillation of individual molecules. This hypothesis should be analyzed more carefully with the further theoretical and experimental analyses. The experimental observations supported the hypothesis that the dynamical state change of the CI, which is driven by the ATPase activity in the CI, is a pacemaker of the oscillation (Terauchi et al., 2007 and Abe et al., 2015), but this hypothesis has not been analyzed theoretically. Therefore, many important problems of the ATPase activity remain to be elucidated, and theoretical models for solving these problems have been much desired and the further comprehensive analyses are required for elucidating the relationship between ATP hydrolysis and the phosphorylation/dephosphorylation rhythm. In this thesis, we developed two theoretical models to examine the mechanism behind this relationship.

1.7 Two new theoretical models

In this study, we aim to understand how the structural change and reactions in KaiC molecules influence the ensemble-level KaiABC circadian oscillation, with a particular emphasis on the reactions of ATP hydrolysis. Therefore, we seek to develop a theoretical method to investigate the mechanism how the atomic structure and reactions generate and modulate the oscillation. To do that, we need to represent the connection between the physical aspects of the microscopic features of the chemical reactions and the resultant oscillation. There are two folds of influences of the microscopic structure and reactions on the oscillation. One way of influence is to affect the oscillation of individual KaiC molecules, as the oscillation in individual molecules is necessary to get the ensemble-level oscillation. The other way of influence is to change the synchronization, as synchronization among many molecules is also essential in the ensemble-level

oscillation. Thus, one way to explain both the aspects is to develop the ensemble model with a microscopic fine resolution in each molecule in the system. However, because such a model is computationally demanding, we rather develop two distinct models and analyze the effects of synchronization as well as individual oscillation separately.

We develop two 'mesoscopic' models of oscillation for bridging the microscopic- and macroscopic-level descriptions; the single-molecule (SM) model and the many-molecule (MM) model. In both models, structure and reactions in individual KaiC molecules are represented by coarse-grained variables. For example, the structure of the *k*th KaiC hexamer is represented by an order parameter, X_k (X in the SM model by dropping the suffix k); the structural transition is described by the change between states with $X_k \approx 0$ and $X_k \approx 1$. In particular, the role of ATP hydrolysis is investigated with these models by considering the effects of ATPase reactions on the structural change; X_k is perturbed by the ATP hydrolysis in these models, and binding/ dissociation reactions, phosphorylation/dephosphorylation reactions, and ATPase reactions are affected by X_k. With the MM model, we analyzed intermolecular and intramolecular dynamics to examine the necessary conditions for the stable ensemble-level oscillation, the mechanism of synchronization, and temperature compensation. In the SM model, more emphasis is placed on the intramolecular dynamics to analyze the origin of oscillation of individual molecules. In this thesis, we discuss the linkage between microscopic and macroscopic oscillations through the combined analyses with the MM and SM models with a particular focus on the role of ATPase reactions.

Two models, the MM and SM models, are complementary to each other. In the MM model, dynamics of many KaiC molecules are analyzed but chemical and structure states of each hexamer are described in a simplified way by using single variables for each hexamer; D_k for the phosphorylation level and X_k for the structure of the kth hexamer. However, each hexamer is

comprised of six subunits and each subunit has two phosphorylation sites. Stochastic fluctuation of individual subunits and fluctuation at two phosphorylation sites should induce noisy disturbance on the behavior of each hexamer, which might prevent the coherent oscillation of the hexamer. Therefore, an important question is to examine whether the coherent oscillation in each single hexamer is indeed realized through the cooperative interactions among subunits; cooperativity of subunits may diminish the noisy fluctuation of individual subunits. Also, the points to be examined are on the roles of two phosphorylation sites in each subunit. In order to analyze these intra-hexamer problems, we discuss the SM model by describing the dynamical change of structure of each of six subunits and phosphorylation of each of 12 phosphorylation sites (two in each of six subunits) in a single KaiC hexamer.

In this dissertation, we focus on studying the mechanism by which the core circadian clockwork of the cyanobacterium works. **Chapter 1** of this dissertation gave a timeline of the important discoveries related to the circadian clock in cyanobacteria. This chapter also introduced the basics of circadian biology relative to the cyanobacterial model system, and discussed the terminologies, characteristics and rules that pertain to the circadian biology. A brief history of the studies about the circadian rhythm in cyanobacteria, biochemical properties, structure, and function of three Kai proteins was discussed. Then, we discussed the study background and the motivation to develop two theoretical models, the MM model and the SM model. **Chapter 2** of this dissertation discusses the MM model of the KaiABC oscillator to analyze the intermolecular dynamics of a macroscopically large number of molecules. The correlation between intra-molecular dynamics and inter-molecular dynamics, which gives rise to the ensemble-level oscillation, is analyzed. This model is also used to examine the mechanism of synchronization and temperature compensation in the ensemble level. A theoretical model of stochastic molecular

process of a single KaiC hexamer has been introduced in **Chapter 3**. We construct the SM model of intra-molecular reactions and structural changes. Intra-molecular dynamics are analyzed to understand the underlying mechanism of the oscillation of individual molecules. Finally, we briefly describe the resulting insights of the MM model and the SM model in **Chapter 4.** We also discuss the direction for the further study in this final chapter of this dissertation.

Chapter 2: The Many-Molecule (MM) model

2.1 Introduction

In order to clarify the mechanism of the KaiABC clock system, it is important to understand the macroscopic synchronization of a large number of molecules. Synchronization of a large number of molecules is necessary to get a coherent oscillation in the ensemble-level. Therefore, in this chapter, we construct a quantitative model of the ensemble of KaiABC oscillators, the many-molecule (MM) model, to understand the mechanism how the microscopic reactions regulate the ensemble-level oscillation. In the MM model, particular emphasis is placed on the ATPase activity of the CI domain of KaiC. The ATPase activity oscillates in a circadian manner and is intrinsically temperature compensated (Terauchi et al., 2007). The frequency (reciprocal of the period) of the phosphorylation cycle is closely correlated with the ATP hydrolysis rate exhibited by KaiC (Terauchi et al., 2007). Thus, this finding indicated that the state change of KaiC driven by the ATPase activity acts as a circadian pacemaker. However, how the ATP hydrolysis regulates the circadian clock remains elusive. Because the ATPase activity is regulated by microscopic molecular state of individual KaiC molecules and the circadian oscillation is realized at the ensemble-level, we expect that the elucidation of the role of the ATPase activity should provide an important clue for understanding how the microscopic reactions regulate the ensemble-level oscillation.

Here, we assume multifold feedback relations among reactions and structural transition in each KaiC molecule and the structure-dependent binding reactions among Kai proteins. As shown in Figure 6, KaiC contains two duplicate domains, N-terminal (CI) and C-terminal (CII) domains

(Iwasaki et al., 1999), and assembles into a hexamer (Mori et al., 2002) by forming the CI-CII double rings (Pattanayek et al., 2004). We denote this KaiC hexamer as C_6.

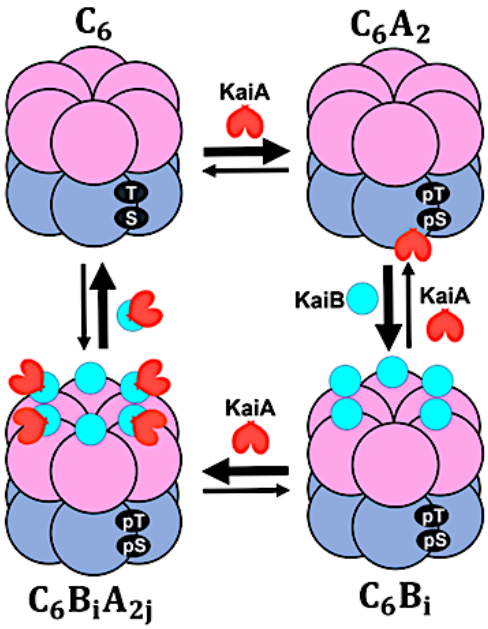

Figure 9: Scheme of interactions among Kai proteins. KaiA dimer (red) binds to the CII domain (blue) to form C_6A_2. KaiB (cyan) binds to the CI domain (pink) of each subunit to form C_6B_i with $1 \leq i \leq 6$ and KaiA dimer further binds to each KaiB to form $C_6B_iA_{2j}$ with $1 \leq j \leq i$. In the CII domain of each subunit, two phosphorylation sites, Ser431 and Thr432 are repeatedly phosphorylated (pS, pT) and dephosphorylated (S, T).

KaiA dimer binds to the CII domain and promotes phosphorylation reactions of KaiC (Xu et al., 2003a). KaiB binds to the CI of each subunit of KaiC hexamer, and a KaiA dimer can further bind to each KaiB to form $C_6B_6A_{2j}$ with $0 \leq j \leq 6$ (Snijder et al., 2017) (Figure 8). The binding of KaiA to the CII is suppressed in forming $C_6B_6A_{2j}$, which promotes the dephosphorylation reactions of

KaiC (Kitayama et al., 2003; Xu et al., 2003a). Thus, the temporal appearance of different kinds of complexes, along with the switching between phosphorylation phase and dephosphorylation phase, is the essential feature of the oscillation in the KaiABC system. As illustrated in Figure 9, we assume that KaiA binds to the CII ring (blue) of KaiC hexamer as a dimer and forms C_6A_2 to stimulate phosphorylation. The CI domain (pink) of each KaiC subunit binds to KaiB (cyan) to form C_6B_i with $1 \leq i \leq 6$. This binding of KaiB promotes dephosphorylation. Then, KaiB further binds to KaiA dimers (red) to form $C_6B_6A_{2j}$ with $0 \leq j \leq 6$.

2.2 Methods

2.2.1 Reactions and structure transition

As explained in the last section, importance of the ATPase activity in the CI domain of KaiC for the ensemble-level oscillation, which was suggested by the experimental reports, is our motivation to develop a theoretical model in this chapter. However, we here do not use this suggested importance in model building, but only assume the possible relations among structure and reactions in individual KaiC molecules and binding/dissociation reactions among KaiA, KaiB, and KaiC molecules, which were inferred from experimental evidences or derived from other biochemical observations. With the model developed with these assumptions, we critically examine how the ATPase activity affects the ensemble-level oscillation. Importance of the ATPase activity for the ensemble-level oscillation is not assumed a priori in model definition but is tested with the simulated results. In this subsection, we explain the assumptions used to develop the MM model.

We describe structure and reactions of individual molecules in a coarse-grained manner and calculate the coupled dynamics of N = 1000 hexamers of KaiC by explicitly following the dynamics of individual hexamers. We assume that KaiA binds as a dimer to the CII domain of KaiC hexamer and form $\mathrm{C_6A_2}$. KaiB monomers bind to the CI domain of each subunit of KaiC hexamer to form $\mathrm{C_6B}_i$ with $1 \le i \le 6$, and KaiA further binds to KaiB to form KaiABC complex, $\mathrm{C_6B}_i\mathrm{A}_{2j}$ with $1 \le j \le i$ (Snijder et al., 2017). The binding/unbinding reactions among Kai proteins are described as

$$\begin{aligned}
&2\mathrm{A} + \mathrm{C_6} \;\rightleftharpoons\; \mathrm{C_6A_2},\\
&\mathrm{B} + \mathrm{C_6B}_i\mathrm{A}_{2j} \;\rightleftharpoons\; \mathrm{C_6B}_{i+1}\mathrm{A}_{2j}, \quad \text{for} \;\; 0 \le i \le 5,\; 0 \le j \le i,\\
&2\mathrm{A} + \mathrm{C_6B}_i\mathrm{A}_{2j} \;\rightleftharpoons\; \mathrm{C_6B}_i\mathrm{A}_{2j+2}, \quad \text{for}\; 1 \le i \le 6,\; 0 \le j \le i-1. \qquad (1)
\end{aligned}$$

In Eq. 1 $\mathrm{C_6B_0A_0}$ is identical to $\mathrm{C_6}$. $P_{C_6A_2}(k,t)$ and $P_{C_6B_iA_{2j}}(k,t)$ denote the probabilities of the kth KaiC hexamer $\mathrm{C_6}$ to be bound in forms of $\mathrm{C_6A_2}$ and $\mathrm{C_6B}_i\mathrm{A}_{2j}$, respectively, with $0 \le i \le 6$ and $0 \le j \le i$ at time t and $k = 1, \dots, N$. Then, the kinetic equation for $P_{C_6A_2}$ is given as

$$\frac{d}{dt}P_{C_6A_2}(k,t) = h_A A^2 P_{C_6B_0A_0}(k,t) - f_A P_{C_6A_2}(k,t), \qquad (2)$$

and the kinetic equation for $P_{C_6B_iA_{2j}}$ can be written with $2 \le i \le 5$ and $1 \le j \le i-1$ as

$$\begin{aligned}
\frac{d}{dt}P_{C_6B_iA_{2j}}(k,t) &= (7-i)h_B B P_{C_6B_{i-1}A_{2j}}(k,t) - (i-j)f_B P_{C_6B_iA_{2j}}(k,t)\\
&\quad - (6-i)h_B B P_{C_6B_iA_{2j}}(k,t) + (i+1-j)f_B P_{C_6B_{i+1}A_{2j}}(k,t)
\end{aligned}$$

$$+ (i-j+1)h_{BA}A^2\, P_{C_6B_iA_{2j-2}}(k,t) - jf_{BA}\, P_{C_6B_iA_{2j}}(k,t)$$

$$- (i-j)h_{BA}A^2 P_{C_6B_iA_{2j}}(k,t) + (j+1)f_{BA}\, P_{C_6B_iA_{2j+2}}(k,t). \qquad (3)$$

Here, $h_A,, h_B,$ and h_{BA} are the binding rate constants and f_A, f_B and f_{BA} are the dissociation rate constants. A and B are the concentrations of unbound free KaiA and KaiB molecules, respectively. In solving Eqs. 2 and 3 numerically, we require the following constraints;

$$P_{C_6A_2}(k,t) + \sum_{i=0}^{6}\sum_{j=0}^{i} P_{C_6B_iA_{2j}}(k,t) = 1, \quad \text{for } k = 1,\dots,N,$$

$$A_T = A + \frac{2}{V}\sum_{k=1}^{N}\left(P_{C_6A_2}(k,t) + \sum_{i=1}^{6}\sum_{j=1}^{i} jP_{C_6B_iA_{2j}}(k,t)\right),$$

$$B_T = B + \frac{1}{V}\sum_{k=1}^{N}\sum_{i=1}^{6}\sum_{j=1}^{i} iP_{C_6B_iA_{2j}}(k,t)\,. \qquad (4)$$

where the total concentrations of KaiA and KaiB are denoted as A_T and B_T respectively, and V is the volume of the system. In the following explanation, we use units with $V = 1$. Because the rate constant of a typical protein dimerization reaction is known to be $\approx \mu\mathrm{M}^{-1}\mathrm{s}^{-1}$ (Northrop & Erickson, 1992), and the typical KaiA concentration prepared in the experiments is around 1 μM, we expect that the dimerization reaction $2\mathrm{A} \rightleftharpoons \mathrm{A}_2$ proceeds in the timescale of seconds or less, which is much faster than the other phosphorylation/dephosphorylation reactions (Nakajima et al., 2010; Murayama et al., 2017; Nakajima et al., 2005) and binding/dissociation occurring more slowly in hours (Chang et al., 2015; Phong et al., 2013). Thus, we assume that dimerization reactions are equilibrated in the solution, and the concentration of A_2 is always proportional to the square of the concentration of A. Therefore, all the reactions involving A_2 are represented in terms of A for the convenience of model description.

We note that Eq. 3 is the expression for the case of $2 \le i \le 5$ and $1 \le j \le i-1$. For the other values of i or j, the corresponding equations are

$$\frac{d}{dt}P_{C_0B_0A_0}(k,t) = -h_A A^2 P_{C_6B_0A_0}(k,t) + f_A P_{C_6A_2}(k,t) - 6h_B B P_{C_6B_0A_0}(k,t) + f_B P_{C_6B_1A_0}(k,t), \quad (5)$$

$$\frac{d}{dt}P_{C_6B_iA_0}(k,t) = (7-i)h_B B P_{C_6B_{i-1}A_0}(k,t) - i f_B P_{C_6B_iA_0}(k,t) - (6-i)h_B B P_{C_6B_iA_0}(k,t) + (i+1)f_B P_{C_6B_{i+1}A_0}(k,t) - i h_{BA} A^2\, P_{C_6B_iA_0}(k,t) - f_{BA}\, P_{C_6B_iA_2}(k,t), \quad \text{for } 1 \le i \le 5 \quad (6)$$

$$\frac{d}{dt}P_{C_6B_iA_{2i}}(k,t) = -(6-i)h_B B P_{C_6B_iA_{2i}}(k,t) + f_B P_{C_6B_{i+1}A_{2i}}(k,t) + h_{BA} A^2\, P_{C_6B_iA_{2(i-1)}}(k,t) - i f_{BA}\, P_{C_6B_iA_{2i}}(k,t), \quad \text{for } 1 \le i \le 5 \quad (7)$$

$$\frac{d}{dt}P_{C_6B_6A_{2j}}(k,t) = h_B B P_{C_6B_5A_j}(k,t) - (6-j)f_B P_{C_6B_6A_{2j}}(k,t) + (7-j)h_{BA} A^2 P_{C_6B_6A_{2(j-1)}}(k,t) - j f_{BA} P_{C_6B_6A_{2j}}(k,t) - (6-j)h_{BA} A^2\, P_{C_6B_6A_{2j}}(k,t) + (j+1)f_{BA}\, P_{C_6B_6A_{2(j+!)}}(k,t), \text{ for } 1 \le i \le 5 \quad (8)$$

$$\frac{d}{dt}P_{C_6B_6A_0}(k,t) = h_B B P_{C_6B_5A_0}(k,t) - 6f_B P_{C_6B_6A_0}(k,t) - 6h_{BA} A^2 P_{C_6B_0A_0}(k,t) + f_{BA} P_{C_6B_6A_2}(k,t), \quad (9)$$

$$\frac{d}{dt}P_{C_6B_6A_{12}}(k,t) = h_{BA} A^2 P_{C_6B_6A_{10}}(k,t) - 6f_{BA} P_{C_6B_6A_{12}}(k,t). \quad (10)$$

In Eqs.1-10, there is no direct KaiC-KaiC interaction, but multiple KaiC hexamers indirectly interact through the dynamical change in concentrations of free unbound KaiA and KaiB. In this model, for a small value of A_T, KaiA is not supplied enough to form C_6A_2 for

phosphorylation, but is consumed to form $C_6B_iA_{2j}$ (Figure 10). This 'sequestration' of KaiA into the $C_6B_iA_{2j}$ complexes brings about the indirect KaiC-KaiC interactions through the depletion of free unbound KaiA. As illustrated in Figure 10, dynamical change of the concentration of free KaiA is important for the indirect KaiC-KaiC interaction, but the dynamical change of free KaiB is not important as discussed later in the Result section.

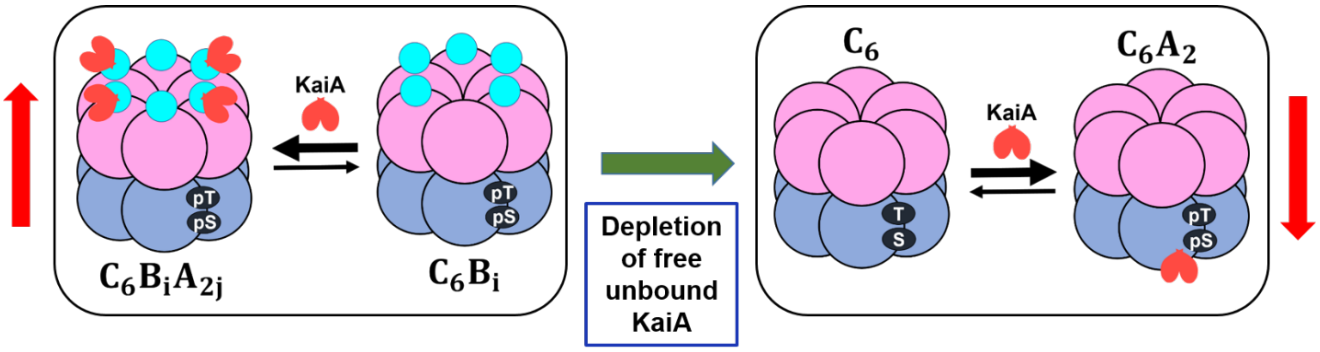

Figure 10: Mechanism of indirect KaiC-KaiC interaction through KaiA sequestration. When the total KaiA concentration is small, consumption of free KaiA is enhanced (upward red arrow) in binding with KaiB of the KaiABC complex, which suppresses (downward red arrow) the binding of KaiA to the CII of the other KaiC through the depletion of free unbound KaiA (green arrow).

Biochemical analysis and structural observations (Chang et al., 2011; Chang et al., 2012; Murayama et al., 2011; Oyama et al., 2016) have revealed that the structure of KaiC hexamer at the unphosphorylated state is more stable and difiifferent from the structure of KaiC hexamer at the phosphorylated state. We assume that a KaiC hexamer takes a tight structure at the unphosphorylated state and a loose structure at the phosphorylated state. We use a continuous

variable X to represent the allosteric transition between tight and loose structural states. We assume that $X_k \approx 1$ when the structure of the kth KaiC hexamer is in the tight structural state, and $X_k \approx 0$ when it is in the loose structural state. We assume that the binding rate constants, h_A and h_B, and the dissociation rate constants, f_A and f_B, should depend on the KaiC structure, $X_k(t)$ as

$$h_A(k,t) = h_A^1 X_k\,, \quad f_A(k,t) = f_A^0(1-X_k),$$
$$h_B(k,t) = h_B^0(1-X_k), \quad f_B(k,t) = f_B^1 X_k, \tag{11}$$

where h_A^1, h_B^0, f_A^0, and f_B^1 are constants. This assumption proposes that KaiA binds to KaiC with higher affinity when the kth KaiC is in the tight structural state. On the other hand, the loose structure of KaiC enhances KaiB binding to the KaiC hexamer. We assume that the binding rate constant, h_{BA}, and the dissociation rate constant, f_{BA}, do not depend on $X_k(t)$ because in forming $C_6B_iA_{2j}$, KaiA binds directly to KaiB and does not to KaiC (Snijder et al., 2017).

We represent the phosphorylation level of twelve sites in a single KaiC hexamer by using a continuous variable. We define $D_k(t) \approx 1$ when the 12 sites of the kth KaiC hexamer are fully phosphorylated, and $D_k(t) \approx 0$ when the 12 sites are fully dephosphorylated. The transition in the phosphorylation level is represented as

$$\frac{dD_k}{dt} = k_p P_{C_6A_2}(k,t) - k_{dp}\left(1 - P_{C_6A_2}(k,t)\right) - \frac{\partial}{\partial D_k} g(D_k). \tag{12}$$

Here, k_p and k_{dp} are rate constants of phosphorylation and dephosphorylation reactions, respectively. The term $g(D) = aD(D-1)(D-1/2)^2$ with $a > 0$ is a constraint for the soft-spin dynamics to restrict the value of D within roughly between 0 and 1 (Sompolinsky & Zippelius.,

1982). We also assume that the structural transition of KaiC between tight and loose states takes place in the time scale of second or less as in typical protein structural transitions, which is much faster than the other phosphorylation/dephosphorylation reactions and binding/dissociation expected in the system. Thus, the structure X_k is represented as a quasi-equilibrium average under the mean-field generated by D_k, the binding probability of KaiA and KaiB, and the effect of ATPase reaction as

$$X_k(t) = \frac{1}{2}\tanh\left[\beta\left(c_0 - c_1 D_k(t) + c_2 p_k^A(t) - c_3 p_k^B(t) - q_k(t)\right)\right] + \frac{1}{2}, \qquad (13)$$

where $\beta = 1/k_B T$ and k_B is the Boltzmann constant, and c_0, c_1, c_2, and c_3 are constants. $p_k^A(t) = P_{C_6A_2}(k,t)$ represents the binding level of KaiA to the kth KaiC hexamer, and the term $p_k^B(t) = \sum_{i=1}^{6}\tanh(i/n_B)\sum_{j=0}^{i} P_{C_6B_iA_{2j}}(k,t)$ is the binding level of KaiB with $n_B = 1$. The term $q_k(t)$ represents the effect of ATPase reactions on the structure.

The term $c_1 D_k(t)$ with $c_1 > 0$ in Eq. 13 gives a negative feedback effect in the system. When D_k is large, KaiC structure tends to stay in the loose structure with small X_k, which lowers the binding affinity of KaiA in Eq.11 and in turn decreases $P_{C_6A_2}(k,t)$ in Eq. 2. Thus, D_k is reduced in Eq. 12. The term $c_3 p_k^B(t)$ with $c_3 > 0$ represents a positive feedback effect. Large $p_k^B(t)$ value and small X_k bring KaiC structure to the loose state, which enhances the binding affinity of KaiB to KaiC through Eq. 11 and increases $P_{C_6B_iA_{2j}}(k,t)$ in Eq. 3. Therefore, the system constitutes multiple feedback interactions. Because of the competitions among multiple feedback interactions, the system tends to stay at the different stationary states. However, the system easily switches

among the states when ATPase reactions add perturbations to produce oscillation in the system. The term $q_k(t)$, representing the effect of ATPase reactions, works as such perturbation.

Earlier experimental data (Chang et al., 2011; Mutoh et al., 2013; Oyama et al., 2016) suggested that the ATP hydrolysis in the CI domain is essential for the association of KaiC to KaiB. This indicates that the ATP hydrolysis induces a structural change of KaiC. We assume that the ATPase reactions take place stochastically in individual CI domains of subunits of each KaiC hexamer with a frequency f_0. We make a simple assumption that $q(i;k,t) = 0$ when ATP is bound or no nucleotide is bound on the CI domain of the ith subunit and $q_k(t) = \sum_{i=1}^{6} q(i;k,t)$ with $q(i;k,t_0) = q_0 \neq 0$ when ATP is hydrolyzed to be ADP and inorganic phosphate (P_i) at time $t = t_0$ in the ith subunit of the kth KaiC hexamer due to the hydrolysis reactions. We consider that the system switches from 0 to q_0 stochastically with the frequency f_0. After this ATP hydrolysis, we assume that ADP is kept bound to the subunit for a time duration δ_k, which is represented by setting $q(i;k,t) = q_0$ for $t_0 \leq t \leq t_0 + \delta_k$ and then ADP is released from the subunit, which makes $q(i;k,t) = 0$. Since ATP is hydrolyzed more frequently during the P-phase (Terauchi et al., 2007), we assume that the ADP release is increased with smaller δ_k and larger X_k. This tendency is represented as the lifetime of the ADP-bound state, δ_k, depends on the hexamer structure,

$$\delta_k = \delta_0 (1 - X_k). \qquad (14)$$

The overall ADP release decreases when δ_k is larger. In our preceding paper (Das et al., 2017), a different parameterization was used in which δ_k was larger than in the present parameterization,

which resulted in the smaller ATPase activity than in this thesis paper, but the qualitative behavior of the model was the same as the present work.

It should be noted that the following is another alternate assumption; $q(i;k,t) = q_0 > 0$ when P_i is released at time $t = t_0$ from the KaiC subunit but ADP is kept bound for the time duration δ_k and $q(i;k,t) = 0$ when ATP is bound, ADP and P_i are bound or no nucleotide is bound on the CI (Das et al., 2017). There is no mathematical difference between this assumption and the assumption made in the last paragraph with the present simplified description of the ATPase reactions in the MM model. We also mention that the model feature remains unchanged even if we assume the alternative mechanism of ATPase reactions with the ADP release prior to the P_i release. The mathematical structure of the model is not changed if we assume that $q(i;k,t) = q_0$ when P_i is kept bound.

ATP hydrolysis takes place mostly in the CI domain whereas phosphorylation/dephosphorylation reactions occur in the CII domain. Thus, allosteric communication between CI and CII is needed to explain the observed effects of ATP hydrolysis on the phosphorylation/dephosphorylation reactions. In the MM model, the term X_k representing the allosteric structural change in Eqs. 11-14 permits such communication.

We solved Eqs. 2-13 numerically to follow the temporal change of $D_k, X_k, P_{C_6A_2}(k,t)$, $P_{C_6B_iA_{2j}}(k,t)$, and $P_{CBA}(k,t) = \sum_{i=1}^{6}\sum_{j=1}^{i} P_{C_6B_iA_{2j}}(k,t)$ with $i = 1,\dots,6$ and $k = 1,\dots,N$ by first discretizing the differential equations and then solving them with a time step of $\Delta t = 0.01$. At every step with $q(i;k,t) = 0$, $q(i;k,t)$ is switched from 0 to $q(i;k,t_0) = q_0 \neq 0$ with the probability of $f_0 \cdot \Delta t$ corresponding to the ATP hydrolysis event. After this switching, $q(i;k,t)$ is kept to be q_0 for the lifetime of δ_k and then switched again to $q(i;k,t) = 0$. Each trajectory consists of

2×10^5 steps corresponding to 2×10^3 h. 10 trajectories are generated with different random numbers, and this set of trajectories are used for the analysis.

Oscillations in the ensemble level are analyzed by calculating the following quantities;

$$\bar{D} = \frac{1}{N}\sum_{k=1}^{N} D_k,$$

$$\bar{X} = \frac{1}{N}\sum_{k=1}^{N} X_k,$$

$$\bar{P}_{C_6A_2} = \frac{1}{N}\sum_{k=1}^{N} P_{C_6A_2}(k,t),$$

$$\bar{P}_{C_6B_iA_{2j}} = \frac{1}{N}\sum_{k=1}^{N} P_{C_6B_iA_{2j}}(k,t),$$

$$\bar{P}_{CBA} = \frac{1}{N}\sum_{k=1}^{N} \bar{P}_{CBA}(k,t). \qquad (15)$$

2.2.2 Temperature dependence of rate constants

One key feature of the KaiABC oscillator is temperature compensation, i.e., the oscillation period remains reasonably stable for a wide range of temperature *in vitro*. The measured value of temperature coefficient, Q_{10} defined by the relative change in the oscillation period upon 10 ℃ temperature change, was about 1.06 (Nakajima et al., 2005) to 1.01 ± 0.02 (Yoshida et al., 2009). However, the physical mechanism of such temperature insensitivity has been elusive. We use the MM model to analyze this problem. We particularly investigate the role of ATP hydrolysis in determining the temperature dependence of the oscillation period and amplitude. In order to test the temperature compensation with the MM model, we define the temperature dependence of rate constants in the model by assuming each of these rates is characterized by activation energy having a reasonable amplitude.

The MM model has nine parameters of rate constants, $h_A^1,\ h_B^0,\ h_{BA},\ f_A^0,\ f_B^1, f_{BA}, a, k_p$, and k_{dp}, and two parameters for the ATP hydrolysis reactions, f_0 and δ_0.We write their values at temperature T around $T_0 = 30°\mathrm{C}$ as

$$h_A^1(T) = [h_A^1(T_0)\exp(\Delta E_{hA}/k_\mathrm{B}T_0)]\exp(-\Delta E_{hA}/k_\mathrm{B}T),$$
$$h_B^0(T) = [h_B^0(T_0)\exp(\Delta E_{hB}/k_\mathrm{B}T_0)]\exp(-\Delta E_{hB}/k_\mathrm{B}T),$$
$$h_{BA}(T) = [h_{BA}(T_0)\exp(\Delta E_{hBA}/k_\mathrm{B}T_0)]\exp(-\Delta E_{hBA}/k_\mathrm{B}T),$$
$$f_A^0(T) = \left[f_A^0(T_0)\exp\left(\Delta E_{fA}/k_\mathrm{B}T_0\right)\right]\exp\left(-\Delta E_{fA}/k_\mathrm{B}T\right),$$
$$f_B^1(T) = \left[f_B^1(T_0)\exp\left(\Delta E_{fB}/k_\mathrm{B}T_0\right)\right]\exp\left(-\Delta E_{fB}/k_\mathrm{B}T\right),$$
$$f_{BA}(T) = \left[f_{BA}(T_0)\exp\left(\Delta E_{fBA}/k_\mathrm{B}T_0\right)\right]\exp\left(-\Delta E_{fBA}/k_\mathrm{B}T\right),$$
$$a(T) = [a(T_0)\exp(\Delta E_a/k_\mathrm{B}T_0)]\exp(-\Delta E_a/k_\mathrm{B}T),$$
$$k_p(T) = \left[k_p(T_0)\exp\left(\Delta E_p/k_\mathrm{B}T_0\right)\right]\exp\left(-\Delta E_p/k_\mathrm{B}T\right),$$
$$k_{dp}(T) = \left[k_{dp}(T_0)\exp\left(\Delta E_{dp}/k_\mathrm{B}T_0\right)\right]\exp\left(-\Delta E_{dp}/k_\mathrm{B}T\right),$$
$$f_0(T) = \left[f_0(T_0)\exp\left(\Delta E_{f0}/k_\mathrm{B}T_0\right)\right]\exp\left(-\Delta E_{f0}/k_\mathrm{B}T\right),$$
$$\delta_0(T) = [\delta_0(T_0)\exp(-\Delta E_{\delta 0}/k_\mathrm{B}T_0)]\exp(\Delta E_{\delta 0}/k_\mathrm{B}T). \quad (16)$$

We compare various cases for the values of eleven activation energies, ΔE_{hA}, ΔE_{hB}, ΔE_{hBA}, ΔE_{fA}, ΔE_{fB}, ΔE_{fBA}, ΔE_a, ΔE_p, ΔE_{dp}, ΔE_{f0}, and $\Delta E_{\delta 0}$;

(I) $\Delta E_{hA} = \Delta E_{hB} = \Delta E_{hBA} = \Delta E_{fA} = \Delta E_{fB} = \Delta E_{fBA}$
$= \Delta E_a = \Delta E_p = \Delta E_{dp} = \Delta E_{f0} = \Delta E_{\delta 0} = 5k_\mathrm{B}T_0,$

(II) $\Delta E_{hBA} = 15k_\mathrm{B}T_0$, Other activation energies $= 5k_\mathrm{B}T_0$,

(III) $\Delta E_{hBA} = \Delta E_{\delta 0} = 15k_{\mathrm{B}}T_0$, Other activation energies $= 5k_{\mathrm{B}}T_0$,

(IV) $\Delta E_{hBA} = \Delta E_{\delta 0} = 15k_{\mathrm{B}}T_0$, and $\Delta E_{f0} = 0$, Other activation energies $= 5k_{\mathrm{B}}T_0$.

(V) $\Delta E_{f0} = 0$, Other activation energies $= 5k_{\mathrm{B}}T_0$,

(VI) $\Delta E_{hBA} = 15k_{\mathrm{B}}T_0$ and $\Delta E_{f0} = 0$, Other activation energies $= 5k_{\mathrm{B}}T_0$. (17)

Here, in the case I, we make the simplest assumption by taking all the relevant activation energies to be same. The stronger temperature dependence of h_{BA}, the binding affinity of KaiA to KaiB, is assumed in the Case II. Hatakeyama and Kaneko (Hatakeyama & Kaneko, 2012) discussed that enhancement of the KaiA sequestration at higher temperature reduces the phosphorylation rate, which should lead to the temperature compensation. In the MM model, this enhancement of KaiA sequestration is represented by the larger ΔE_{hBA} than others. The important features of the MM model are the dependence of the oscillation period on the frequency of the ATP hydrolysis f_0 and on the lifetime of the ADP binding state δ_0 as shown in Results section. In case III, the stronger temperature dependence of δ_0 is also assumed with the larger $\Delta E_{\delta 0}$. In this case, the rate of ADP release is enhanced with increased temperature, and δ_0 becomes small with the larger temperature dependence than other reactions. The frequency of ATP hydrolysis was shown to be temperature insensitive (Terauchi et al., 2007). Though the precise mechanism of this temperature insensitivity has not been known, a possible explanation for this temperature insensitivity is the regulation of the reaction rate by the diffusive non-activation type binding process of ATP to the CI. Here, we represent this temperature insensitivity by further assuming $\Delta E_{f0} = 0$ in the case IV. The effects of the assumption $\Delta E_{f0} = 0$ is checked in the Cases V and VI.

2.2.3 Parameters in the MM model

We assume that the phosphorylation/dephosphorylation reactions are slow enough with the rates k_p ~ 0.5-1 h^{-1} and k_{dp} ~ 0.5-1 h^{-1} to realize the period ~24 hour of the phosphorylation/dephosphorylation rhythm (Phong et al., 2013). The timescale of ATPase reactions, ${f_0}^{-1}$ and δ_k, should be also as slow as f_0 ~ 1-2 h^{-1} and δ_k~ 0.5-1 hour. This estimated slow rates of ATPase reactions are consistent with the structural observation (Abe et al., 2015). We assume that the binding/dissociation rates of KaiA and KaiB defined as $h_A A^2$,$h_{BA} A^2$,$h_B B$, f_A, f_{BA}, and f_B should be h^{-1}- min^{-1}; such slow binding/dissociation of KaiB is consistent with the observed data (Chang et al., 2015; Phong et al., 2013). We found that the ensemble oscillation in the MM model is stable for the wide range of parameter values with this rough estimation of parameter values, but we should note that the simulated period of oscillation depends on the parameter. Because different experimental conditions showed different values of the period from 22 h to 26 h (Nakajima et al., 2010; Murayama et al., 2017; Nakajima et al., 2005), we do not calibrate the parameters to reproduce a particular experimental report. Thus, we use a typical set of parameters to grasp the important features of the oscillation. An example parameter set is summarized in Table 1. Unless otherwise mentioned, we discuss the results calculated with this parameter set in Results section.

The total concentrations of KaiA and KaiB, A_T and B_T, are set to $2\,N/V$ and $20\,N/V$, respectively in Table 1. In monomer basis, this corresponds to the concentration ratio of $\mathrm{KaiA:KaiB:KaiC} = 1:10:3$. In many *in vitro* experimental measurements, the ratio was set to $\mathrm{KaiA:KaiB:KaiC} = 1:3:3$ (Nishiwaki et al., 2007; Terauchi et al., 2007), and the effects of varying these concentrations were tested by Nakajima et al. (Nakajima et al., 2010). They showed that the oscillation amplitude and period were not changed when the KaiB concentration was

varied between KaiA: KaiB: KaiC $= 1:3:3$ and $1:15:3$ (Nakajima et al., 2010). The values used for A_T and B_T in Table 1 fall in this range. Values in Table 1 are shown with units of $V = 1$. Alternatively, by using units of $V = 3 \times 10^{-15}\ l$, the concentration of KaiC is $6N/V \approx 3.3$ μM with $N = 1000$. This value is close to 3.5 μM which is the value often used in *in vitro* experiment for the KaiC concentration (Terauchi et al., 2007; Nakajima et al., 2010). A typical value of KaiB binding rate constant, which is $h_B^0 = 2 \times 10^{-6}\ \mathrm{h}^{-1}$ with units of $V = 1$ is $h_B^0 = (6.02 \times 10^{23}) \times (3 \times 10^{-15})\ \mathrm{M}^{-1} \times (2 \times 10^{-6}\ \mathrm{h}^{-1}) \approx 3.6 \times 10^{3}\ \mathrm{M}^{-1}\mathrm{h}^{-1}$ with units of $V = 3 \times 10^{-15}\ l$. This value should be directly compared with the observed data when the experimental data of KaiB monomer kinetics becomes available.

Table 1. Parameters in the MM model

Rate constant of KaiA binding to KaiC	h_A^1	6.6×10^{-6} h^{-1}	Max. lifetime of ADP binding after hydrolysis	δ_0	2.6 h
Rate constant of KaiB binding to KaiC	h_B^0	2×10^{-6} h^{-1}	Effect of ATP hydrolysis on structure	q_0	$k_\mathrm{B}T_0$ *
Rate constant of KaiA binding to KaiB	h_{BA}	1.8×10^{-6} h^{-1}	Base-line temperature effect on structure	c_0	$10k_\mathrm{B}T_0$ *
Rate constant of KaiA dissociation from KaiC	f_A^0	6×10^{-1} h^{-1}	Effect of phosphorylation on structure	c_1	$8k_\mathrm{B}T_0$ *
Rate constant of KaiB dissociation from KaiC	f_B^1	4×10^{-1} h^{-1}	Effect of KaiA binding on structure	c_2	0
Rate constant of KaiA dissociation from KaiB	f_{BA}	2×10^{-1} h^{-1}	Effect of KaiB binding on structure	c_3	$4k_\mathrm{B}T_0$ *
Constant for variable confinement	a	2.2 h^{-1}	Total copy number of KaiA monomers	A_T	$2N$
Rate constant of phosphorylation	k_p	4.4×10^{-1} h^{-1}	Total copy number of KaiB monomers	B_T	$20N$
Rate constant of dephosphorylation	k_{dp}	4.4×10^{-1} h^{-1}	Total copy number of KaiC hexamers	N	1000
Frequency of ATP hydrolysis	f_0	2.2 h^{-1}	System volume	V	1

*$T_0 = 30$ °C

2.3 Results

2.3.1 Oscillation in ensemble of KaiC hexamers

An example of the ensemble-level oscillation simulated with the MM model is shown in Figure 11a. The oscillation of the KaiC phosphorylation level, $\overline{D}(t)$, the structure of KaiC hexamers, $\bar{X}(t)$, the probability of C_6 of forming the C_6A_2 complex, $\bar{P}_{C_6A_2}$, and probability of forming the $C_6B_iA_{2j}$ complexes, $\bar{P}_{CBA}(t)$, are shown where overbars represent that averages were taken over the ensemble of N = 1000 hexamers as defined in Eq. 15. Here, $\bar{P}_{C_6A_2}(t)$ and $\bar{P}_{CBA}(t)$ show counter-phased oscillation. When $\bar{P}_{C_6A_2}(t)$ dominates, binding of KaiA to KaiC hexamer enhances phosphorylation. As a result of this domination of $\bar{P}_{C_6A_2}(t)$, $\overline{D}$ is increased and $\bar{X}$ is decreased. On the contrary, when $\bar{P}_{CBA}(t)$ is large, KaiA is sequestered into $C_6B_iA_{2j}$, which depletes the free unbound KaiA. Hence, there are not sufficient free KaiA molecules to form C_6A_2, which then decreases $\overline{D}$ and increases $\overline{X}$. Individual KaiC hexamers communicate with each other through this sequestration of KaiA, which is necessary for the ensemble-level oscillation (Figure 10).

In Figure 11b, individual oscillation of single KaiC hexamer are shown. Here, oscillation trajectories of $D_k(t)$, $X_k(t)$, $P_{C_6A_2}(k,t)$ and $P_{CBA}(k,t)$ of a KaiC hexamer, which was arbitrarily chosen from the ensemble, are plotted. In the phosphorylation phase, the lifetime of bound ADP, δ_k, becomes short with large $X_k(t)$, and ADP is frequently released from the CI. This short residence of ADP at CI does not have much effect on $X_k(t)$. However, when $X_k(t)$ begins to be small, δ_k becomes longer and ATP hydrolysis provides higher influence to $X_k(t)$. This gives rise to spike-like changes in $X_k(t)$, which induces a noisy fluctuating decrease of $D_k(t)$. This

fluctuation is smoothed out when averaged over a large number of KaiC hexamers, which gives rise to a coherent oscillation of $\overline{D}$.

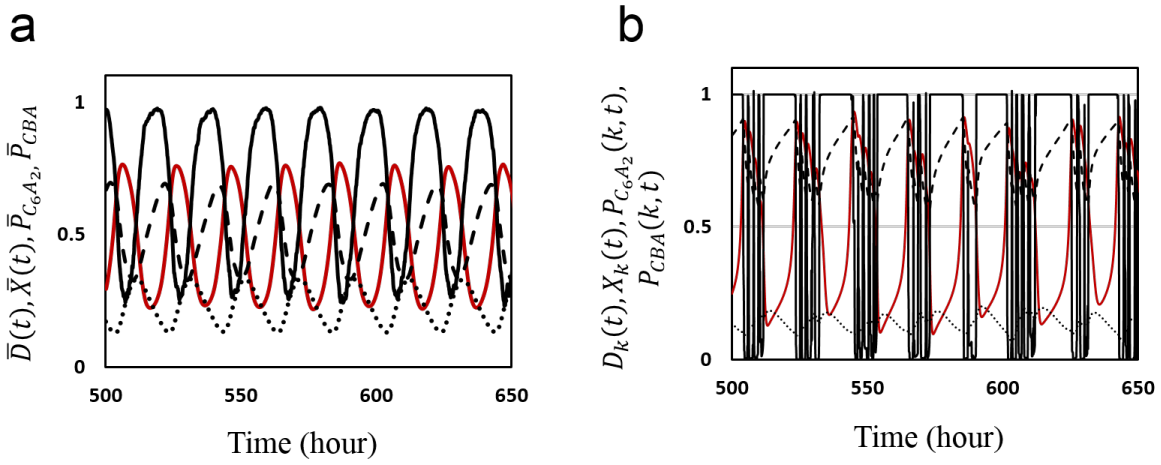

Figure 11: Simulated ensemble and single molecule oscillations with the MM model. **a**) The ensemble oscillation of the phosphorylation level $\overline{D}(t)$ (red line), structure of KaiC hexamer $\bar{X}$ (t) (black real line), probability to form complex $\mathrm{C_6A_2}$, $\bar{P}_{C_6A_2}$(dashed line), and probability to form complexes $\mathrm{C_6B_iA_{2j}}$, $\bar{P}_{CBA}$ (dotted line), are shown by plotting averages over the ensemble of N = 1000 hexamers as functions of time. **b**) The single molecule oscillation of phosphorylation level $D_k(t)$ (red line), structure $X_k(t)$ (black real line), $P_{C_6A_2}(k,t)$ (dashed line), $P_{CBA}(k,t)$ (dotted line) of a KaiC hexamer arbitrarily chosen from the ensemble are plotted as functions of time. Parameters in Table 1 were used. Here, overbars represent the ensemble average of quantities as defined in Eq.15.

2.3.2 Synchronization of KaiC molecules

To analyze the synchronization shown in Figure 11 furthermore, we plot together the ensemble-averaged oscillation $\overline{D}(t)$ and individual oscillations $D_k(t)$ of five KaiC hexamers arbitrarily chosen from *N* hexamers. Parameter values in Table 1 were used to plot individual and ensemble oscillations in Figure 12a. In this case, fluctuations among individual oscillations are synchronized and entrained into the ensemble oscillation, which gives rise to a stable coherent oscillation of the ensemble. The essential role of KaiA sequestration in this synchronization is clearly shown in Figure 12b. In this figure, free KaiA concentration is fixed to be $A = 0.2A_T$. When the free KaiA concentration is constant as in Figure 12b, the sequestration mechanism does not work and individual KaiC hexamers lose synchronization among them. Then, the ensemble-level oscillation disappears though individual molecules show oscillation with the large amplitude. Thus, dynamical change of free KaiA concentration generates the temporal change of the binding rate of KaiA to KaiC, $h_A A^2$, which is essential for maintaining the synchronization. In contrast, both synchronization and the ensemble oscillation are maintained when the free KaiB concentration is fixed to be $B = 0.9B_T$ as shown in Figure 12c. This maintenance of synchronization among individual oscillations shows that the temporal change in the concentration of free KaiB is not necessary for synchronization.

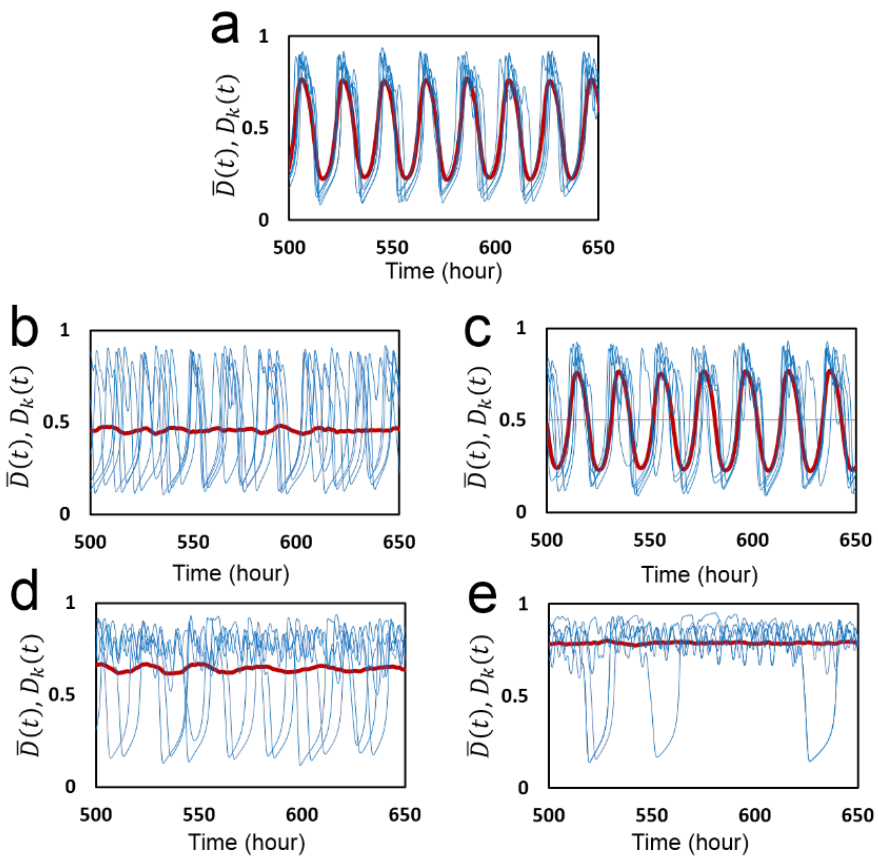

Figure 12: Simulated oscillations of individual molecules and the ensemble-averaged oscillation. The phosphorylation oscillation $D_k(t)$ (blue) of five individual KaiC hexamers, which are arbitrarily selected from the ensemble of N=1000 hexamers, are superposed with the ensemble-averaged oscillation $\overline{D}(t)$ (red). **a**) Parameters in Table 1 were used with f_0 = 2.2 h^{-1}. **b**) The concentration of free KaiA is set constant to be $A = 0.2A_T$ but the concentration of KaiB is changing dynamically. **c**) The concentration of free KaiB is set constant to be $B = 0.9B_T$ but the concentration of KaiA is changing dynamically. The frequency of ATP hydrolysis is changed to **d**) f_0 = 0.8 h^{-1} and **e**) f_0 = 0.5 h^{-1}.

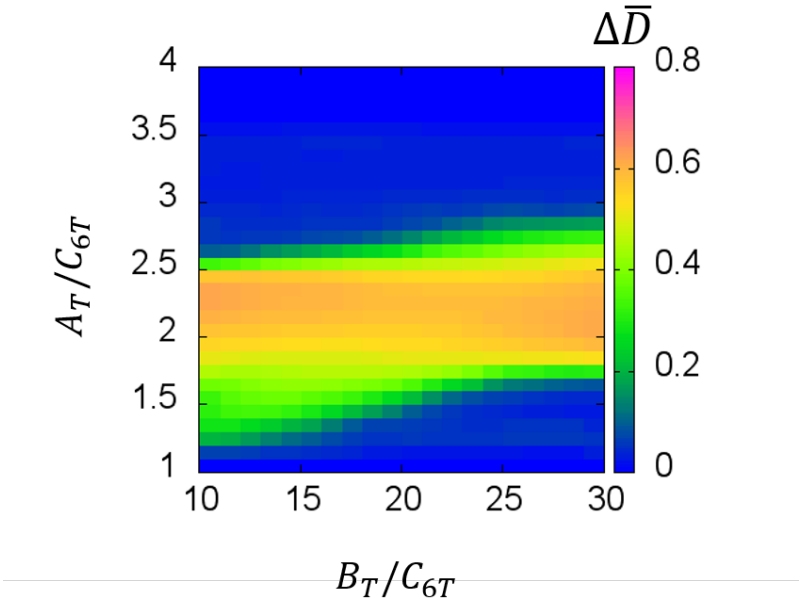

Figure 13: The oscillation amplitude $\Delta\overline{D}$ of phosphorylation level $\overline{D}(t)$. $\Delta\overline{D}$ is plotted on the plane of A_T/C_{6T} and B_T/C_{6T}. KaiA concentration A_T and KaiB concentration B_T are normalized by KaiC concentration C_{6T}.

Dependence of the ensemble-level oscillation on concentrations of KaiA and KaiB is shown in Figure 13 by plotting amplitude of oscillation, $\Delta\overline{D}$. When the KaiA concentration is larger than a threshold of $A_T/C_{6T} \approx 1.5$, $\Delta\overline{D}$ becomes large. However, the sequestration mechanism does not work and the synchronization is lost to make $\Delta\overline{D} \approx 0$ when KaiA concentration is large. On the other hand, the upper limit of the KaiB concentration for the proper oscillation was not found within the reasonable range since the sequestration mechanism is not working for KaiB. Existence of such concentration ranges of KaiA and KaiB agrees with the experimental observation (Nakajima et al., 2010).

It is interesting to see how the ATP hydrolysis affects the synchronization since ATP hydrolysis shows a significant role to generate individual oscillations in Figure 11b. In Figure 12d, individual and ensemble oscillations are calculated with the ATP hydrolysis frequency, $f_0 = 0.8\ \mathrm{h}^{-1}$, which is smaller than the ATP hydrolysis frequency $f_0 = 2.2\ \mathrm{h}^{-1}$, used in Figure 12a. We find synchronization is lost with this small frequency of ATP hydrolysis. Therefore, ATP hydrolysis with sufficient frequency is necessary for maintaining synchronization. ATP hydrolysis occurring with random timing in individual KaiC subunits should perturb each KaiC hexamer to adjust to the dynamical oscillation of free KaiA concentration; without this adjustment, individual KaiC hexamers stay oscillating with their own individual phases. By further reducing the ATP hydrolysis frequency to $f_0 = 0.5\ \mathrm{h}^{-1}$ in Figure 12e, many KaiC hexamers stop oscillating and show small amplitude fluctuation. Therefore, when f_0 decreased, KaiC oscillators first lose synchronization and then lose individual oscillations.

Together, these results showed that in the MM model KaiA sequestration is a basis for synchronization of individual KaiC hexamers, and ATP hydrolysis helps individual KaiC hexamers to synchronize under the mechanism of KaiA sequestration.

2.3.3 Effects of ATPase activity on the oscillation

Since ATP hydrolysis helps to bring oscillation in individual molecules and also plays an important role in maintaining synchronization, it is interesting to see how ATP hydrolysis drives the circadian oscillations. The effects of ATPase reactions are analyzed by varying q_0, δ_0, and f_0, which are the parameters to define the ATPase reactions in the MM model. Figure 14 shows variation of the simulated trajectories when the degree of influence of ATPase reaction to the structure, q_0, is changed. When q_0 is too small, ATPase reactions do not have sufficient impact

for perturbing the system from the steady state with large $\overline{X}$ and large $\overline{D}$. However, when q_0 too large, ATPase reactions stabilize the (large $\overline{X}$, small $\overline{D}$) state and prevents oscillation. This is summarized by plotting the oscillation amplitude, $\Delta\overline{D}$, and the oscillation period, τ in Figure 15a. τ is defined by $\tau = 1/f_p$ with f_p being the frequency of the peak of Fourier transformed spectrum of $\overline{D}(t)$, where the Fourier transform of $\overline{D}(t)$ was calculated by Fast Fourier Transform algorithm, in which 2×10^3 h long trajectory is discretized into 2×10^5 steps, and then averaged over 10 trajectories. $\Delta\overline{D}$ becomes large only when q_0 exceeds a certain threshold and $\Delta\overline{D}$ remains non-zero within a certain range of q_0. τ is decreasing with the large value of q_0. Figure 15b shows $\Delta\overline{D} \neq 0$ when the lifetime of ADP bound state, δ_0, remains within a limited range. When δ_0 is too small, the (large $\overline{X}$ and large $\overline{D}$) state is stabilized, and when δ_0 is too large, the (large $\overline{X}$ and small $\overline{D}$) state is stabilized, which prevents the system from oscillation with frequent ATPase reactions. As shown in Figure.15a, $\Delta\overline{D}$ shows two peaks at $q_0 = 1.0$ and $q_0 = 1.65$. The reason for these perceptible peaks can be confirmed by observing the calculated trajectories as shown in Figures 16a and 16b. In Figure 16a, oscillation of $\overline{X}$ is smooth at $q_0 = 1.0$. On the other hand, at $q_0 = 1.65$, oscillation of $\overline{X}$ shows a saturation with $\overline{X} \approx 1$ in the phosphorylation phase and drops sharply in the dephosphorylation phase as shown in Figure. 16b. This result suggests that there are two slightly different oscillation modes in the present model and the significance of these two modes are altered at the threshold of $q_0 \approx 1.2$ where the oscillation of $\overline{X}$ is smooth. We also find two peaks at $\delta_0 = 2.6$ and $\delta_0 = 5.0$ in Figure 15b. Two oscillation modes are found in Figure 16c and Figure 16d, which are the oscillation trajectories calculated at these two peaks. At the threshold $\delta_0 \approx 3.6$, these two modes are switched from one to the other.

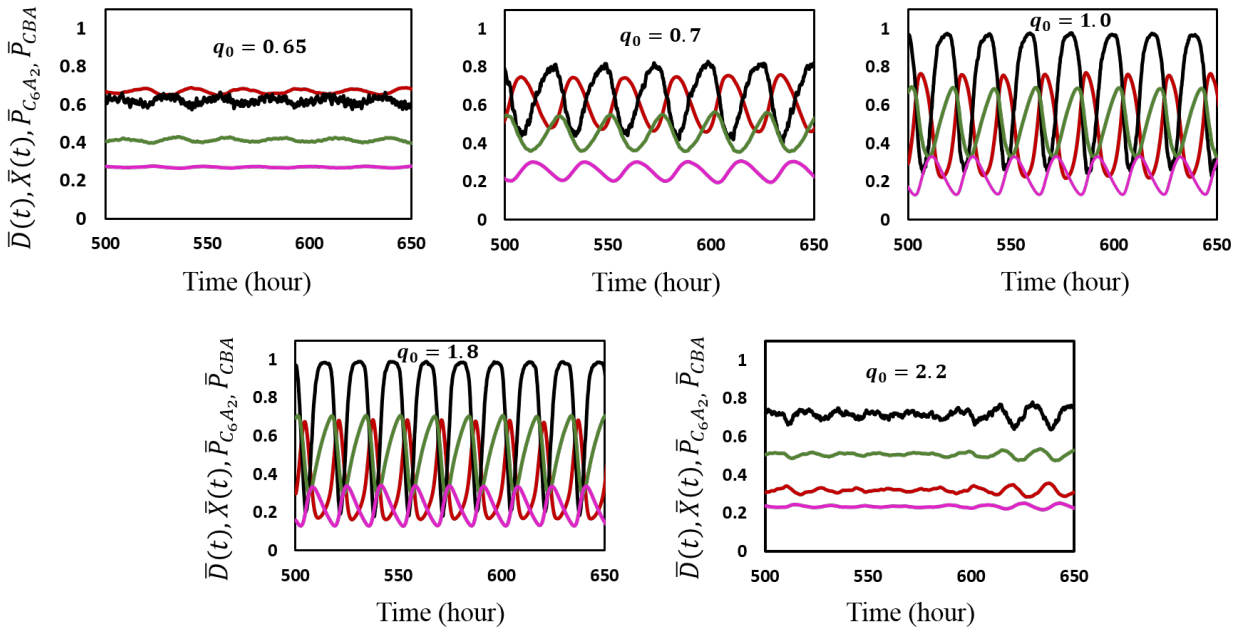

Figure 14: Example trajectories calculated with different values of q_0. The ensemble averages of KaiC phosphorylation level $\bar{D}$ (red), KaiC hexamer structure $\bar{X}$ (black), the probability of forming the C_6A_2 complex, $\bar{P}_{C_6A_2}$ (green), and the probability of forming the $C_6B_iA_{2j}$ complexes, $\bar{P}_{CBA}$ (pink), are plotted as functions of time. The value of q_0 is written in units of k_BT_0 in each panel. Values in Table 1 were used for parameters other than q_0.

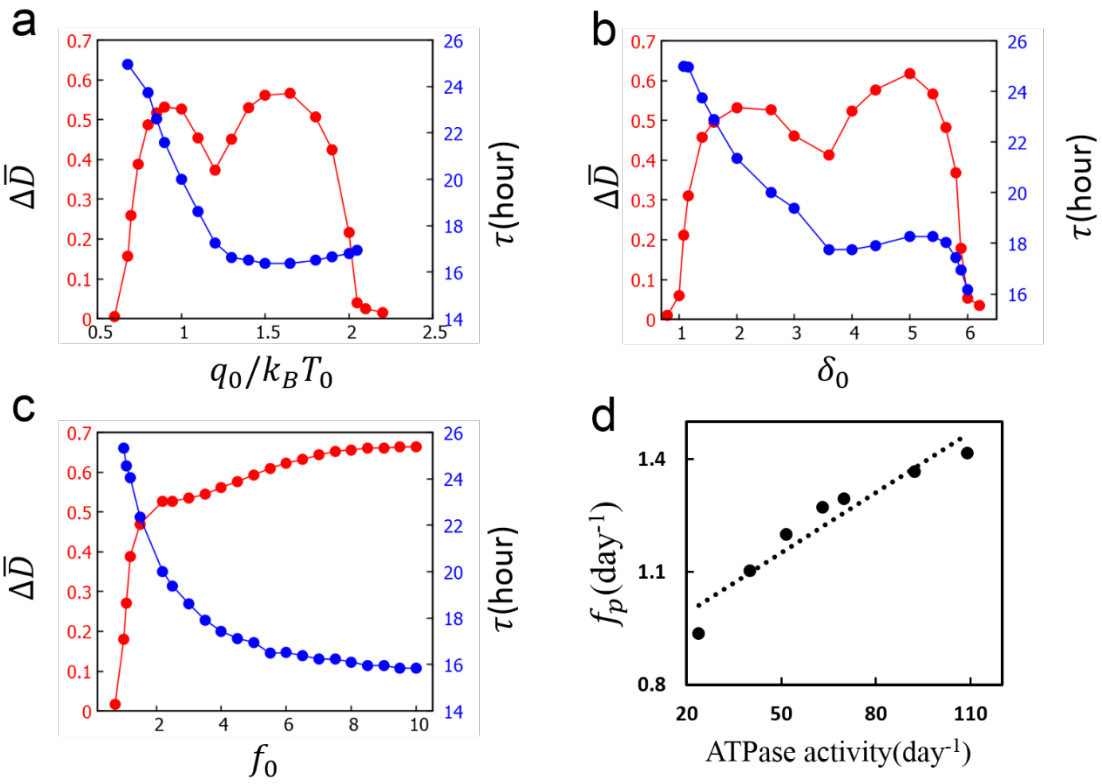

Figure 15: Effects of ATPase reactions on the circadian oscillation of the Kai system. **a**–**c**) The oscillation amplitude $\Delta\bar{D}$ (red) and the oscillation period τ (blue) are plotted by varying the values of **a**) the amplitude of impact of the ADP bound state on the structure, q_0 , **b**) the lifetime of the ADP bound state, δ_0, and **c**) the frequency of the ATPase reactions, f_0. **d**) The correlation between ATPase activity and the oscillation frequency is shown by plotting the simulated results for $f_0 =$ 1.0 h^{-1}, 1.7 h^{-1}, 2.3 h^{-1}, 2.7 h^{-1}, 3.0 h^{-1}, 4.0 h^{-1} and 5.0 h^{-1}. The ATPase activity was calculated in the non-oscillatory condition and the oscillation frequency of the average phosphorylation level, $\bar{D}$, f_p, was calculated in the oscillatory condition. Parameters used are the same as Table 1 except for those varied in each graph. Each point is the average of 10 trajectories, each having 2×10^3 h length.

When the frequency of ATP hydrolysis f_0 is larger than a certain value, the oscillation amplitude $\Delta\overline{D}$ becomes large as shown in Figure 15c. When f_0 is large enough, frequent ATPase reactions stabilize the oscillation around the (large $\overline{X}$ and large $\overline{D}$) state. Thus, the system shows saturation with too large f_0. τ is decreasing with increasing value of f_0.

Summarizing Figures 15a-c, the steady state turns into oscillation when the quantities that define the ATPase reactions in the model, q_0 , δ_0 and f_0, are larger than certain thresholds. Hence, in the present model, ATP hydrolysis, which is randomly processed in individual CI domains, is a driving mechanism of the ensemble-level oscillation.

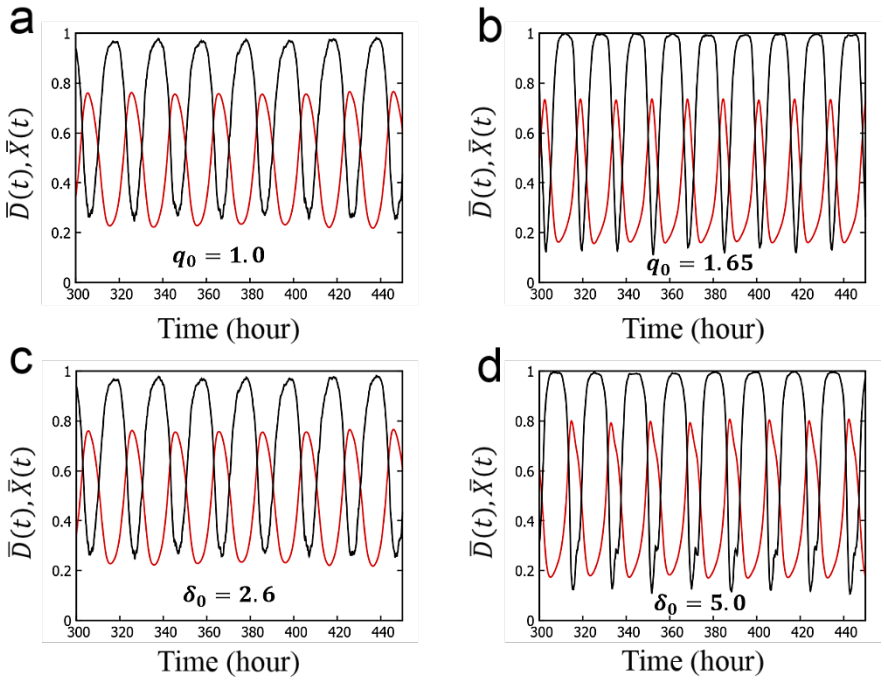

Figure 16: Example trajectories of phosphorylation level of $\overline{D}(t)$ (red line) and structure of KaiC hexamer $\overline{X}$ (t) (black line) are plotted with **a**) q_0 =1.0, **b**) q_0 =1.65, **c**) δ_0 = 2.6 and **d**) δ_0 = 5.0.

The oscillation period is also modulated by changes in q_0, δ_0 and f_0 as shown in Figure 15a-c. In addition, the ATPase activity of KaiC, which is obtained by averaging the number of released ADP from each CI domain in 24 h in the non-oscillatory condition of $A_T = B_T = 0$ for $f_0 =$ 1.0 h^{-1}, 1.7 h^{-1}, 2.3 h^{-1}, 2.7 h^{-1}, 3.0 h^{-1}, 4.0 h^{-1} and 5.0 h^{-1}, is also sensitively dependent on f_0. In Figure 15d, the thus calculated ATPase activity is compared with the frequency f_p of phosphorylation rhythm calculated in the oscillatory condition with A_T/N=2 and B_T/N =20. We find a clear correlation between ATPase activity and f_p. Though the number of released ADP shown here is larger than the experimentally observed value of (3-20) ADP/day/KaiC (Abe et al., 2015; Terauchi et al., 2007), the calculated amount of the released ADP is close to the experimental data in our published paper (Das et al., 2017) where a different parameter set was used and the similar correlation between the oscillation frequency and the ATPase activity was found. Thus, the perturbation of structure by the ATPase reactions in individual molecules is a key determinant of the oscillation frequency in the ensemble of many molecules.

2.3.4 Temperature compensation

To investigate the role of ATP hydrolysis on the temperature insensitivity of the circadian oscillation, in Figure 17a and Figure 17b, the temperature dependences of period and amplitude of the ensemble-averaged oscillation $\overline{D}(t)$ are calculated for cases I-VI defined in Eq.17 of the Method section. As shown in Figure 17a, there are only small differences between case I and case II and between case V and case VI. Therefore, the enhancement of KaiA sequestration at higher temperature contributes only slightly to bring temperature compensation of period in the present model. This ineffectiveness of KaiA sequestration to temperature compensation is consistent with the simulated results in the present model, showing that the free KaiA concentration does not much

affect the oscillation period. On the other hand, period calculated in cases III and IV is much more insensitive to temperature than period calculated in cases I and II. This result indicates that the intense temperature dependence of the lifetime of the ADP bound state gives a significant effect for the temperature compensation. Temperature insensitivity of ATP hydrolysis frequency also gives some effect to make period insensitive to temperature as shown in the differences between case III and case IV and between II and VI in Figure 16a. Q_{10} of the oscillation frequency calculated between 30°C and 40°C is $Q_{10} = 1.17$ (case I), 1.16 (case II), 1.07 (case III), and 1.02 (case IV),1.13 (case V), and 1.10 (case VI).

The simulated results on the importance of the lifetime of the ADP bound state for temperature compensation could be interpreted as in the following manner: As shown in Figure 11b, the structure of a KaiC hexamer is not much affected by ATP hydrolysis when X_k is large and the lifetime of the ADP bound state δ_k becomes small through Eq. 14. We refer to the ATP hydrolysis reactions which give a sufficient impact to the structure as 'effective ATP hydrolysis'. Therefore, the frequency of the effective ATP hydrolysis decreases and the frequency of ineffective ATP hydrolysis increases as δ_0 decreases. Because the oscillation frequency is correlated to the frequency of the ATP hydrolysis as shown in Figure 15d, we can expect that the decrease in the effective frequency of ATP hydrolysis decreases the oscillation frequency and compensates acceleration of other reactions, leading to the temperature compensation. A possible molecular mechanism of the intense temperature dependence of the lifetime of the ADP bound state is the large activation energy of molecular gating that opens/closes a pathway for the ADP to be expelled from the KaiC. This hypothesis could be checked experimentally by comparing mutants of amino acid residues near the ADP discharge pathway, which should change the lifetime of the ADP bound state.

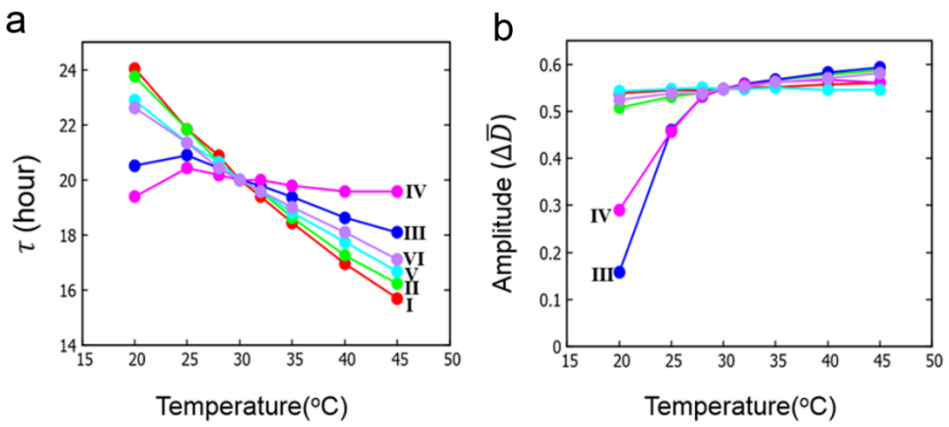

Figure 17: Temperature dependence of **a**) Period τ and **b**) amplitude $\Delta\overline{D}$ of the ensemble oscillation $\overline{D}(t)$ of the KaiC phosphorylation. Six cases are compared: case I (red), case II (green), case III (blue), case IV (magenta), case V (cyan), and case VI (purple). Cases I-VI are explained in Eq. 17. Parameters in Table 1 were used.

The amplitude of oscillation becomes only slightly small as temperature decreases in cases I, II, V, and VI as shown in Figure 17b. However, in cases III and IV, the amplitude approaches rapidly to 0 as the temperature is decreased. In cases III and IV, the oscillation amplitude continuously decreases and vanishes at a certain threshold temperature. In other words, the oscillation disappears with the Hopf bifurcation mechanism in low temperature, which is the behavior consistent with the experimental observation (Murayama et al., 2017).

Summarizing these results of Figure 17a and 17b, we found that the enhanced release of ADP from the CI with increased temperature largely contributes to temperature compensation of oscillation period, and insensitivity of ATP hydrolysis frequency to temperature also gives some help to temperature compensation. The prolonged release of ADP at low temperature is consistent

with the observed disappearance of oscillation through the Hopf bifurcation at low temperature (Murayama et al., 2017). Meanwhile, enhancement of KaiA sequestration does not help much for temperature compensation.

2.4 Summary of the analyses with the MM model

The MM model is a coarse-grained model of the reconstituted circadian clock. This model explains oscillation dynamics of an ensemble of a large number of Kai molecules and the dynamics of the constituent individual molecules. In this model, we assumed that the binding affinity of KaiA and KaiB to KaiC depends on the structure of KaiC hexamers and the rates of phosphorylation/dephosphorylation depend on whether KaiA is bound or not. ATPase activity was assumed to depend on the structure of KaiC and the ATPase reactions bring perturbation on the allosteric transition of the KaiC structure.

Simulations with the MM model showed that stochastic individual oscillations are synchronized through the communication among KaiC hexamers, which is realized by the sequestration of KaiA into the KaiABC complex, and the ATPase reactions in the CI domain perturb individual KaiC hexamers to allow them to generate the ensemble level oscillation when the ATPase reactions are more frequent than a threshold frequency. Thus, both KaiA sequestration and frequent ATPase reactions perform pivotal roles to maintain a coherent ensemble-level oscillation. Temperature dependence of the period and amplitude of the ensemble-level oscillation were examined with the MM model, and it was shown that the intense temperature dependence of the lifetime of the ADP bound state in the CI domain is important to realize the temperature compensation of the oscillation period, and such dependence of the lifetime of the ADP bound state is consistent with the observed disappearance of oscillation at low temperature (Murayama

et al., 2017). It was also shown that temperature insensitivity of the frequency of ATP hydrolysis helps temperature compensation to some extent.

Chapter 3: The Single-Molecule (SM) model

3.1 Introduction

KaiC is a hexameric protein and each of its subunits shows very slow and stable ATPase activity. A key observation is a clear correlation between the ATPase activity of KaiC and the phosphorylation rhythm (Terauchi et al., 2007), which suggested that the dynamic state change of KaiC driven by ATP hydrolysis is a pacemaker of the oscillation. In the previous chapter, the MM model was developed for testing this hypothesis at the ensemble level. However, with the MM model, we analyzed the dynamical behavior of a large number of KaiC molecules by describing each hexamer with single variables, and questions on the intra-hexamer dynamics remain unclear: How do the interactions among subunits of each hexamer generate the coherent oscillation in the hexamer, and how do the two phosphorylation sites in each subunit contribute to the oscillation of the hexamer? In order to solve these problems of intra-hexamer fluctuations and oscillations, the theoretical analyses of more details of reactions and structural changes with the single-molecule (SM) modeling are necessary. As shown in Figure 12b, synchronization of many KaiC hexamers is lost when the concentration of free KaiA is kept constant, but the amplitude of the oscillation of individual KaiC hexamers is kept large. In order to analyze the problem of how the oscillation of single individual hexamers is maintained, we use the simple assumption of the constant free KaiA concentration in the SM model. This corresponds to the situation that the total KaiA concentration in the system is large, so that the change in the free KaiA concentration is negligible. With this assumption, synchronization is lost, which results in the diminishment of the ensemble-level oscillation, but this assumption is enough for analyzing the condition of how the oscillation in the single KaiC hexamer is realized.

In the SM model, we follow the hypothesis that KaiC goes through an allosteric transition between tight and loose structure and the transition is induced by the change in the phosphorylation state of KaiC.

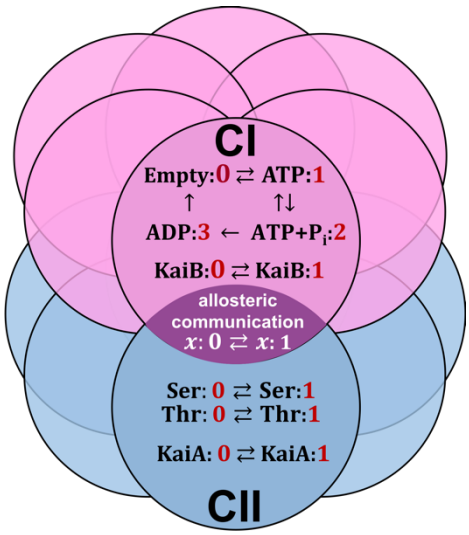

Figure 18: Reactions and states in each KaiC subunit in the SM model. ATP hydrolysis reactions and KaiB binding/dissociation reactions occur in the CI domain (pink). Phosphorylation/dephosphorylation reactions and KaiA binding/dissociation reactions take place in the CII domain (blue). CI and CII domains are coupled through allosteric structural change. A single hexamer formed by six subunits is considered in the SM model.

Rates of the phosphorylation/dephosphorylation reactions, on the other hand, should depend on the structure of KaiC. The allosteric transition changes the binding affinities of KaiA and KaiB to KaiC, thereby changes the rates of phosphorylation/dephosphorylation reactions. Therefore, modulation in the phosphorylation/dephosphorylation reactions and the allosteric structure change form feedback loops. ATPase activity through binding, hydrolysis, and release of nucleotide

modulates the KaiC structure, thereby modulates the feedback relation between the phosphorylation/dephosphorylation reactions and the structure transition. In this Chapter, we describe this feedback mechanism in the single-molecular level. As shown in Figure 18, we assume that in each subunit of a single KaiC hexamer, phosphorylation/dephosphorylation reactions and KaiA binding/dissociation reactions occur in the CII domain whereas ATPase reactions and KaiB binding/dissociation reactions occur in the CI domain. The reactions in the CI domain and the CII domain are coupled through the allosteric structural change.

3.2 Methods

3.2.1 Reactions and structure transition

In the SM model, each subunit of a hexamer switches between two conformational states; $x_i = 0$ when the *i*th subunit is in the loose structural state and $x_i = 1$ when it is in the tight structural state with $i = 1, \dots, 6$. Though both CI and CII domains can bind ATP, we focus on the ATPase activity in the CI domain because ATP hydrolysis is dominantly taking place in the CI domain (Terauchi et al., 2007). The four nucleotide binding states in the CI domain of the *i*th subunit are represented as $a_i = 0$ when no nucleotide is bound, $a_i = 1$ when ATP is bound, $a_i = 2$ when ADP and P_i are bound, and $a_i = 3$ when P_i is released and ADP is kept bound. As shown in Figure 18, we define variables, Ser_i and Thr_i, as $Ser_i = 1$ ($Thr_i = 1$) when Ser431 (Thr432) of the *i*th subunit is phosphorylated and $Ser_i = 0$ ($Thr_i = 0$) when Ser431 (Thr432) of the *i*th subunit is dephosphorylated. We write $KaiA = 1$ when a KaiA dimer binds to the CII ring and $KaiA = 0$ when a KaiA dimer dissociates from the CII ring. We write $KaiB_i = 1$ when a KaiB monomer binds to the *i*th subunit and $KaiB_i = 0$ when a KaiB monomer dissociates from the *i*th subunit. Thus, as shown in Figure 18, the states of six subunits in a single KaiC hexamer are

described by the variable $KaiA$ and others;

$$\text{States of KaiC subunits} = KaiA, \{KaiB_i,\ a_i,\ Ser_i, Thr_i, x_i\} \text{ with } i = 1,\ldots,6. \qquad (18)$$

For the reason that the atomic structure is rapidly changing with the time scale of milliseconds or shorter but other variables should change more slowly in minutes or longer time scales, we describe the free energy G of the KaiC hexamer as a function of $\{x_i\}$ as $G = G(x_1, x_2, \ldots, x_6)$;

$$G(x_1, x_2, \ldots\ldots, x_6) = \sum_{i=1}^{6} x_i \left[b_0 + b_1^{Thr} Thr_i + b_1^{Ser} Ser_i - b_2\, KaiA + b_3\, KaiB_i - b_4\, \theta(a_i)\right] - J \sum_{i=1}^{6} \left(x_i - \frac{1}{2}\right)\left(x_{i+1} - \frac{1}{2}\right), \qquad (19)$$

Here, $b_0, b_1^{Thr}, b_1^{Ser}, b_2, b_3, b_4$, and J are constants. In the last term of equation, $x_7 = x_1$. If we regard the fast varying quantities $\{x_i\}$ as 'spin variables', G of Eq. 19 should correspond to the 'effective Hamiltonian' for spins, where the slow variables, Thr_i, Ser_i, $KaiA$, $KaiB_i$ and $\theta(a_i)$ correspond to the magnetic fields acting on the spins. In other words, phosphorylation states, binding states, and ATPase states give biases for the structural change of each KaiC subunit. The term $x_i b_4 \theta(a_i)$ represents coupling between ATPase reactions and structure. Here, we assume that $\theta(a_i) = -1$ when $a_i = 2$ or 3, $\theta(a_i) = 1$ when $a_i = 1$, and $\theta(a_i) = 0$ when $a_i = 0$. These assumptions indicate that the binding of ATP increases the tendency of KaiC hexamer structure to be tight while the binding of ADP+Pi or ADP loosens the structure. Here, J represents coupling between two neighbor subunits; $J > 0$ implies that subunits change their structures in a cooperative way to give rise to two-state allosteric structural transition of the KaiC hexamer.

For the timescale of minutes, we can represent the structural state of each KaiC subunit with a quasi-equilibrium thermal average of x_i as

$$\langle x_i \rangle = \mathrm{Tr}\, x_i \exp(-\beta G)\, /Z \qquad (20)$$

by approximately treating Thr_i, Ser_i, $KaiA$, $KaiB_i$ and $\theta(a_i)$ as stationary variables, where Tr represents a sum over all possible values of $\{x_i\}$ and Z is a partition function, $Z = \mathrm{Tr} \exp(-\beta G)$. Then, we represent the hexamer state by using the following variables;

$$Ser = \frac{1}{6}\sum_{i=1}^{6} Ser_i\,, \qquad Thr = \frac{1}{6}\sum_{i=1}^{6} Thr_i,$$

$$X = \tfrac{1}{6}\textstyle\sum_{i=1}^{6}\langle x_i \rangle\,, \quad D = \tfrac{1}{2}(Ser + Thr), \qquad (21)$$

where X and D are the average structural state and the average phosphorylation level respectively.

By comparing Eqs. 13 and 19, we find that b_0, b_1^{Thr} and b_1^{Ser}, b_2, b_3, and b_4 in the SM model correspond to c_0, c_1, c_2, c_3, and q_0 in the MM model, respectively. Thus, we find Eq.19 provides multiple feedback relations in the SM model. When $b_2 > 0$, binding of KaiA brings KaiC structure to the tight state as it decreases the energy G, which increases the binding affinity of KaiA to KaiC and enhances phosphorylation. When $b_3 > 0$, binding of KaiB brings the structure of KaiC into the loose state. This effect is consistent with the mass spectrometry observation (Snijder et al., 2014) and enhances dephosphorylation, which further increases the binding affinity of KaiB. Therefore, the terms in Eq. 19, $b_2 > 0$ and $b_3 > 0$ provide positive feedback effects in the system. On the other hand, the $b_1^{Ser} > 0$ term stabilizes the loose structure of the KaiC subunit

with phosphorylation state of Ser431 by lowering the energy G, which reduces the binding affinity of KaiA and stimulates dephosphorylation of Ser431. Hence, the $b_1^{Ser} > 0$ term provides a negative feedback effect in the system. We assume $b_1^{Thr} < b_1^{Ser}$ to make the phosphorylation of Thr432 faster than the phosphorylation of Ser431. This assumption is consistent with the experimental observation (Nishiwaki et al., 2007; Rust et al., 2007). In this model, our assumption is $b_1^{Thr} < 0 < b_1^{Ser}$. The $b_1^{Thr} < 0$ term stabilize the tight structure of KaiC which increase the binding affinity of KaiA and thus, stimulates phosphorylation of Thr432. Therefore, the $b_1^{Thr} < 0$ term gives a positive feedback effect. As a result of the coexistence of these multiple feedback relations, the system has two metastable states: the phosphorylated loose-structure state and the dephosphorylated tight-structure state. Because of the competition between the two states, the system makes transitions between them. Here, ATPase reactions add perturbation to the structure and stimulate the transition between them. The term $x_i b_4 \theta(a_i)$ in Eq. 19 represents such perturbation through the ATPase reactions into the system.

The binding/dissociation reactions of KaiA occur in the CII ring of KaiC hexamer. The reactions are defined as

$$KaiA = 0 \overset{h_a}{\rightarrow} KaiA = 1,\ KaiA = 1 \overset{f_a}{\rightarrow} KaiA = 0\ . \tag{22}$$

Our assumption is that the structure of KaiC hexamer, which undergoes the allosteric structural change, controls the binding affinity of KaiA to KaiC. The tight structure of hexamer enhances the binding of KaiA whereas the loose structure suppresses the binding of KaiA. To represent this assumption, we consider that the rates in Eq. 22 are regulated by X as

$$h_a = h_a^1 X, \qquad f_a = f_a^0 (1 - X). \tag{23}$$

A constant h_a^1 should depend on the concentration of free unbound KaiA molecules. Here in the present SM model, we make a simple assumption that the free KaiA concentration is constant to keep h_a^1 constant. This assumption represents the situation that the KaiA concentration is much larger than the KaiC concentration so that the free KaiA concentration is not affected by the oscillation of individual KaiC molecules. In the MM model, as shown in the subsection 2.3.2, sequestration of KaiA to $C_6B_iA_{2j}$ and the resultant temporal depletion of free KaiA concentration is the mechanism of synchronization among multiple KaiC hexamers and synchronization is lost when the free KaiA concentration is kept constant. We here adopt a simple assumption that h_a^1 is kept constant as synchronization mechanism is not discussed with the SM model.

The binding/dissociation reactions of KaiB in the CI domain of KaiC hexamer are described as

$$KaiB_i = 0 \xrightarrow{h_{b_i}} KaiB_i = 1, \quad KaiB_i = 1 \xrightarrow{f_{b_i}} KaiB_i = 0. \tag{24}$$

The rates in Eq. 24 are assumed to be regulated by the structure of subunits $\langle x_i \rangle$ in the following manner;

$$h_{b_i} = h_b^0(1 - \langle x_i \rangle), \qquad f_{b_i} = f_b^1 \langle x_i \rangle , \tag{25}$$

With this hypothesis, the tight structure of the *i*th subunit of KaiC reduces the binding affinity of KaiB to the subunit while the loose structure of the subunit increases the KaiB binding affinity. Again, we use a simplified assumption that h_b^0 is kept constant through the simulation time course.

The phosphorylation/dephosphorylation reactions in the CII domain are described by

$$Ser_i = 0 \xrightarrow{k_{i,0\to1}^{Ser}} Ser_i = 1, \quad Ser_i = 1 \xrightarrow{k_{i,1\to0}^{Ser}} Ser_i = 0,$$

$$Thr_i = 0 \xrightarrow{k_{i,0\to1}^{Thr}} Thr_i = 1, \quad Thr_i = 1 \xrightarrow{k_{i,1\to0}^{Thr}} Thr_i = 0. \tag{26}$$

The rates in Eq. 26 are regulated by the binding status of KaiA as

$$k_{i,0\to1}^{Ser} = k_{0\to1}^{Ser,1} KaiA + k_{0\to1}^{Ser,0} (1 - KaiA),$$

$$k_{i,1\to0}^{Ser} = k_{1\to0}^{Ser,1} KaiA + k_{1\to0}^{Ser,0} (1 - KaiA),$$

$$k_{i,0\to1}^{Thr} = k_{0\to1}^{Thr,1} KaiA + k_{0\to1}^{Thr,0} (1 - KaiA),$$

$$k_{i,1\to0}^{Thr} = k_{1\to0}^{Thr,1} KaiA + k_{1\to0}^{Thr,0} (1 - KaiA). \tag{27}$$

We assume the following six equations for the change of nucleotide binding state;

$$a_i = 0 \xrightarrow{k_{i,01}^{a}} a_i = 1, \quad \text{ATP binding}$$

$$a_i = 1 \xrightarrow{k_{i,10}^{a}} a_i = 0, \quad \text{ATP unbinding}$$

$$a_i = 1 \xrightarrow{k_{i,12}^{a}} a_i = 2, \quad \text{hydrolysis reaction}$$

$$a_i = 2 \xrightarrow{k_{i,21}^{a}} a_i = 1, \quad \text{backward reaction}$$

$$a_i = 2 \xrightarrow{k_{i,23}^{a}} a_i = 3, \quad \text{P}_\text{i} \text{ release}$$

$$a_i = 3 \xrightarrow{k_{i,30}^{a}} a_i = 0. \quad \text{ADP release} \tag{28}$$

Here, both the forward and backward reactions are considered for binding/unbinding of ATP and ATP hydrolysis. Binding reaction of P_i or ADP is not considered by assuming that their concentrations are small. The rates in Eq. 28 are assumed to depend on the structure of each subunit $\langle x_i \rangle$ as in the following manner;

$$k^{a}_{i,01} = k^{a,1}_{01}\langle x_i\rangle + k^{a,0}_{01}(1 - \langle x_i\rangle),$$

$$k^{a}_{i,10} = k^{a,1}_{10}\langle x_i\rangle + k^{a,0}_{10}(1 - \langle x_i\rangle),$$

$$k^{a}_{i,12} = k^{a,1}_{12}\langle x_i\rangle + k^{a,0}_{12}(1 - \langle x_i\rangle),$$

$$k^{a}_{i,21} = k^{a,1}_{21}\langle x_i\rangle + k^{a,0}_{21}(1 - \langle x_i\rangle),$$

$$k^{a}_{i,23} = k^{a,1}_{23}\langle x_i\rangle + k^{a,0}_{23}(1 - \langle x_i\rangle),$$

$$k^{a}_{i,30} = k^{a,1}_{30}\langle x_i\rangle + k^{a,0}_{30}(1 - \langle x_i\rangle). \quad (29)$$

Here, $k^{a}_{i,01}$, $k^{a}_{i,10}$, $k^{a}_{i,12}$, $k^{a}_{i,21}$, $k^{a}_{i,23}$, and $k^{a}_{i,30}$ are dynamical variables, while $k^{a,1}_{01}$, $k^{a,0}_{01}$, $k^{a,1}_{10}$, $k^{a,0}_{10}$, $k^{a,1}_{12}$, $k^{a,0}_{12}$, $k^{a,1}_{21}$, $k^{a,0}_{21}$, $k^{a,1}_{23}$, $k^{a,0}_{23}$, $k^{a,1}_{30}$, and $k^{a,0}_{30}$ are constant parameters.

We perform numerical simulations of the stochastic dynamics in the SM model by combining the calculation with the Gillespie algorithm (Gillespie, 1977) and the quasi-equilibrium calculation of $\langle x_i\rangle$ and X of each subunit. The Gillespie algorithm is a sort of the Monte Carlo algorithm in the sense it uses random numbers, but differs from the Metropolis algorithm based on the energy calculation. In the Metropolis algorithm, some trial movement of the system is generated in each step and that trial is accepted or rejected as a movement to define the next step depending on the energy change caused by the trial. On the other hand, in the Gillespie algorithm, the system is moved at every time, or in other words, all the movements or reactions generated by random numbers are accepted. Here, the choice of both reaction type and the length of time step (waiting time for the reaction) depend on the rates of reactions defined in the model. Therefore, the Gillespie algorithm is efficient to simulate chemical reactions because there is no rejection or waste of the generated movements (or reactions) and is used as a standard method in simulating the non-equilibrium process of chemical reactions.

The procedure of the calculation in the SM model is summarized in Figure 19. At Step 0, we set values for the parameters in Eq. 19 and Eqs. 22-29 and initialize values of $KaiA$, $KaiB_i$, a_i, Ser_i, and Thr_i at $t = 0$. Then, $\langle x_i \rangle$ and X are calculated with Eq. 19 and the rates of reactions are calculated with Eqs. 22-29 at Step 1.

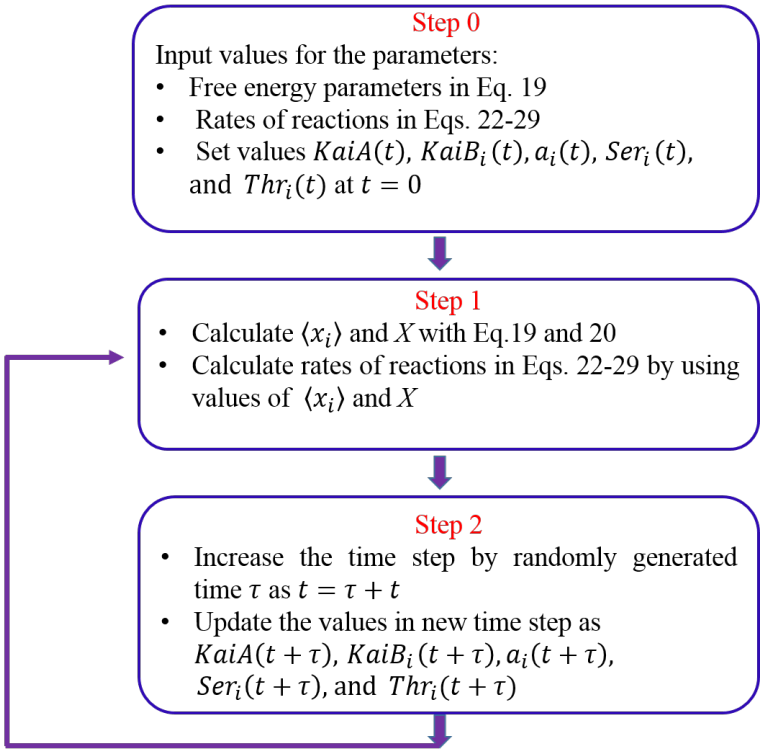

Figure 19: Schematic of the calculation procedure in the SM model. After defining parameters and initial values in Step 0, the structure of each subunit $\langle x_i \rangle$ and their hexameric average X are calculated with the quasi-equilibrium approximation, and the rates of reactions are calculated in Step 1. Then, by using these reaction rates, one particular reaction is chosen to update the state variables and the width of time step is determined by using the Gillespie algorithm in Step 2. By using the thus updated state variables, $\langle x_i \rangle$, X, and the reaction rates in the new step are calculated in Step 1. The cycle from Step 1 to Step 2 is iterated to obtain the system trajectory.

After that, in Step 2, the time is increased by a step width τ as $t = t + \tau$, where τ is generated at each step by using a random number from an exponential distribution. Next, one of the all possible reactions is randomly chosen with the probability proportional to the reaction rates of Eqs. 23, 25, 27 and 29, and $KaiA,\ KaiB_i, a_i,\ Ser_i,$ or Thr_i are updated accordingly (Gillespie, 1977). Then, by using the thus updated $KaiA,\ KaiB_i, a_i,\ Ser_i,$ or Thr_i, Step 1 is performed again and the structural variables $\langle x_i \rangle$ and X in the new time step is calculated with Eq. 19 and 20. The cycle from Step 1 to Step 2 is iterated until the number of steps exceeds a predefined number that limits the length of a trajectory in the calculation. Through the iterations from Step 1 to Step 2, we obtain trajectories for $KaiA,\ KaiB_i,\ a_i,\ Ser_i,$ and Thr_i from the initial condition defined in Step 0.

To obtain the oscillation frequency from the calculated trajectory, we performed the fast Fourier transformation (FFT) of $D(t)$. To perform the FFT, a sequence of the data sampled with a constant width of time step Δt are necessary. However, in the Gillespie algorithm, time steps are not equidistant because each step width is determined to fit the exponential distribution defined by the rate constants in the model, and this fitting is realized by generating a random number in each step. Therefore, as explained in Figure 20, to perform the FFT of $D(t)$, we mapped the sequence of variable time steps generated by the Gillespie algorithm to the sequence of constant time steps.

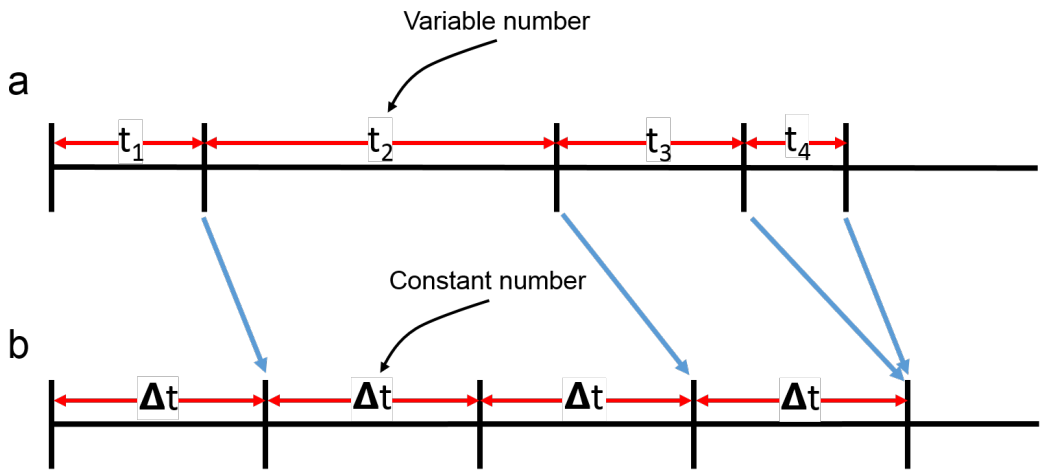

Figure 20: Illustration of the mapping of time steps. **a**) Each time step in a simulated trajectory is random variable number generated from an exponential distribution. **b**) The sequence of constant time steps. A constant width Δt is the average length between steps determined as the ratio of the total time length of the trajectory to the number of the reaction steps in the trajectory generated with Gillespie algorithm.

3.2.2 Parameters in the SM model

Parameters in the SM model were set to have the same order of magnitude as the corresponding parameters in the MM model. In the SM model, more detailed reaction schemes are considered, so that the larger number of parameters are defined than in the MM model. For example, the phosphorylation/dephosphorylation reactions are considered at two sites, Ser431 and Thr432, which are regulated by the binding status of KaiA. Therefore, the rates of the phosphorylation/dephosphorylation reactions are defined by two sets of parameters, those in the KaiA bound state, $k_{0\to1}^{Ser,1}$, $k_{1\to0}^{Ser,1}$, $k_{0\to1}^{Thr,1}$, $k_{1\to0}^{Thr,1}$, and those in the KaiA unbound state, $k_{0\to1}^{Ser,0}$, $k_{1\to0}^{Ser,0}$, $k_{0\to1}^{Thr,0}$, $k_{1\to0}^{Thr,0}$. Here, superscripts 1 and 0 imply the rates in the KaiA bound and

unbound states, respectively. We consider that the phosphorylation rates are larger in the KaiA bound state and the dephosphorylation rates are larger in the KaiA unbound state. Therefore, $k_{0\to1}^{Ser,1}, k_{0\to1}^{Thr,1} > k_{0\to1}^{Ser,0}, k_{0\to1}^{Thr,0}$ and $k_{1\to0}^{Ser,1}, k_{1\to0}^{Thr,1} < k_{1\to0}^{Ser,0}, k_{1\to0}^{Thr,0}$. Because the phosphorylation/dephosphorylation reactions at Thr432 precedes the phosphorylation/dephosphorylation reactions at Ser431, we consider $k_{0\to1}^{Thr,1} > k_{0\to1}^{Ser,1} > k_{1\to0}^{Thr,1} > k_{1\to0}^{Ser,1}$ and $k_{1\to0}^{Thr,0} > k_{1\to0}^{Ser,0} > k_{0\to1}^{Thr,0} > k_{0\to1}^{Ser,0}$. In addition, we assume ATP hydrolysis rates depend on the structure of each subunit; the reaction rates are larger when the structure is tight. Therefore, we assume $k_{01}^{a,1}$, $k_{10}^{a,1}$, $k_{12}^{a,1}$, $k_{21}^{a,1}$, $k_{23}^{a,1}$, and $k_{30}^{a,1}$ are larger than $k_{01}^{a,0}, k_{10}^{a,0}, k_{12}^{a,0}, k_{21}^{a,0}, k_{23}^{a,0}$, and $k_{30}^{a,0}$. Here, superscripts 1 and 0 indicate the rates in the tight and loose structures, respectively. An example parameter set, the parameters of rate constants and the parameters in the free energy to determine the structure, is summarized in Tables 2 and 3.

Table 2. Rate constants in the SM model*

ATP hydrolysis reactions in the tight structure	$k_{01}^{a,1}$	1.1	Phosphorylation/dephosphorylation reactions with KaiA unbound from KaiC	$k_{0\to1}^{Thr,0}$	0.3
	$k_{10}^{a,1}$	1.0		$k_{1\to0}^{Thr,0}$	3.9
	$k_{12}^{a,1}$	1.1		$k_{0\to1}^{Ser,0}$	0.01
	$k_{21}^{a,1}$	1.0		$k_{1\to0}^{Ser,0}$	0.5
	$k_{23}^{a,1}$	1.1	Phosphorylation/dephosphorylation reactions with KaiA bound to KaiC	$k_{0\to1}^{Thr,1}$	4.8
	$k_{30}^{a,1}$	1.1		$k_{1\to0}^{Thr,1}$	0.2
ATP hydrolysis reactions in the loose structure	$k_{01}^{a,0}$	0.55		$k_{0\to1}^{Ser,1}$	0.6
	$k_{10}^{a,0}$	0.5		$k_{1\to0}^{Ser,1}$	0.1
	$k_{12}^{a,0}$	0.55	Binding and dissociation rates of KaiA	h_a^1	1.5
	$k_{21}^{a,0}$	0.5		f_a^0	0.1
	$k_{23}^{a,0}$	0.55	Binding and dissociation rates of KaiB	h_b^0	1.5
	$k_{30}^{a,0}$	0.55		f_b^1	0.2

*Values are in units of h^{-1}.

Table 3. Free energy parameters in the SM model *

Base-line temperature effect	b_0	0.13	Effect of KaiB binding	b_3	1
Effect of Thr432 phosphorylation	b_1^{Thr}	–1	Effect of ATP hydrolysis	b_4	4
Effect of Ser431 phosphorylation	b_1^{Ser}	6	Coupling between subunits	J	4.5
Effect of KaiA binding	b_2	1.5			

*Values are in units of $k_{\mathrm{B}}T_0$ with $T_0 = 30$ °C.

3.3 Results

3.3.1 Oscillation in individual KaiC hexamer

In Figure 21, the simulated phosphorylation levels, *D*, *Ser*, and *Thr*, and structure *X* of a single KaiC hexamer are plotted; these quantities are defined in Eq. 21 in the subsection 3.2.1. In Figure 21a we find that the phosphorylation level and structure oscillate with opposite phases; this feature is similar to the oscillation in the MM model (Figure 11). From the simulated oscillation of *Ser* and *Thr* in Figure 21b, we find that the phase of *Thr* precedes the phase of *Ser*. In this way, the simulated single-molecular oscillation represents the important features which are observed in the ensemble-level oscillation though it shows noisy stochastic oscillation. Thus, the physical origin of features of the ensemble-level oscillation exists at the single-molecular level.

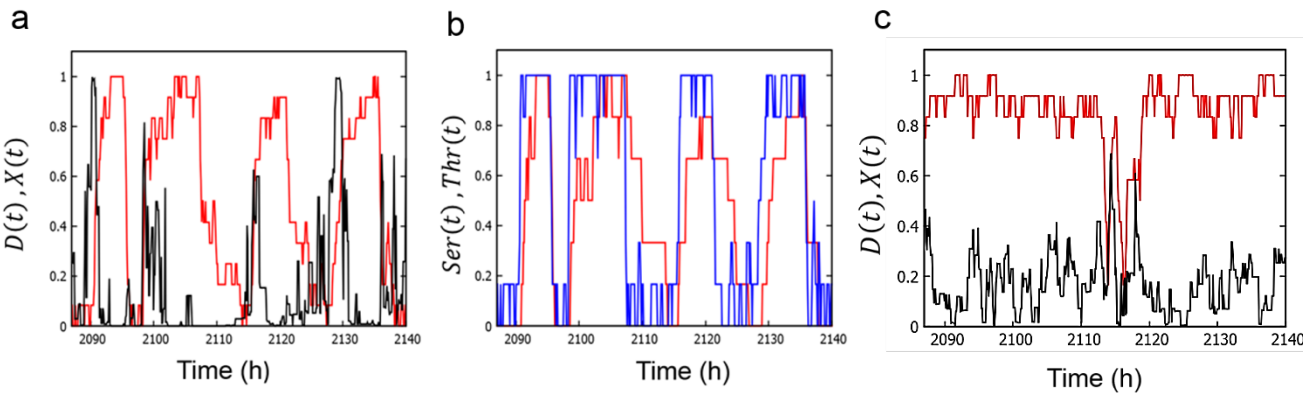

Figure 21: Simulated oscillations of single KaiC hexamer in the SM model. **a**) Oscillation of the phosphorylation level $D(t)$ (red) and structure $X(t)$ (black). **b**) Oscillation of phosphorylation at Ser432 (red) and Thr431 (blue). **c**) Oscillation of the phosphorylation level $D(t)$ (red) and structure $X(t)$ (black) when $J = 0$. Parameters in Tables 2 and 3 were used other than J in **c**.

We should note that among four choices of signs of b_1^{Thr} and b_1^{Ser} in Eq. 19; (+ +), (+ −), (− +), and (− −), one choice of (− +) explained the observed phase difference of phosphorylation oscillation at *Ser* and *Thr* as shown in Figure 21b. As explained in Section 3.2.1, $b_1^{Thr} < 0$ gives a positive feedback effect and $b_1^{Ser} > 0$ gives a negative feedback effect in the model. Therefore, the comparison of the simulated results of the SM model with the experimentally observed oscillations provided insights on how the balance between positive and negative feedback effects is determined in a single KaiC hexamer.

In order to obtain a coherent oscillation as shown in Figure 21a, noisy fluctuations of individual subunits need to be suppressed through the cooperative interactions among subunits. The source of cooperative interactions among subunits of a single KaiC hexamer is the J term in Eq. 19. Indeed, by setting $J = 0$, the oscillation of phosphorylation level $D(t)$ disappeared as shown in Figure 21c. Therefore, the results of the SM model confirmed that the structural communication that brings about cooperativity of subunits is necessary for achieving the coherent oscillation in single KaiC hexamer. The KaiC mutants having different residues at the interface of subunits may correspond to the cases with different J in the present model; therefore, the comparison with the simulated results in varying J with observations of various mutants would give useful insights on the mechanism of how the coherent oscillation is generated at the single-molecular level.

3.3.2 The strength of coupling between reactions and structural change

The mechanism of this single-molecular oscillation can be more closely analyzed by modulating the parameters, b_1^{Thr}, b_1^{Ser}, b_2, b_3, and b_4 in Eq. 19, which represent the strength of coupling between reactions and structural changes. We plot the oscillation amplitude, δD, in Figure 22. We

introduce scaling factors α_1, α_2, and α_3 to scale the parameters as $b_1^{Ser} \rightarrow \alpha_1\, b_1^{Ser}$ (Figure 22a), $b_1^{Thr}, b_2, b_3 \rightarrow \alpha_2\, b_1^{Thr}, \alpha_2\, b_2, \alpha_2 b_3$ (Figure 22b), and $b_4 \rightarrow \alpha_3 b_4$ (Figure 22c). Here, $\delta D = 2 \times$ (standard deviation of the distribution of D), where the values of D were sampled from the trajectory $D(t)$. 2^{24} data points with regular steps mapped from calculated 2^{24} reaction steps as explained in Figure 20. As discussed in the subsection 3.2.1, α_1 modulates the strength of negative feedback interaction between phosphorylation/dephosphorylation reactions and structure, α_2 modulates the strength of positive feedback interactions between phosphorylation/dephosphorylation reactions and structure or between binding and structure, and α_3 modulates the effect of the ATPase reactions on the structure. δD drops to a small value with small α_1 in Figure 22a. This appreciable decrease of δD can be confirmed by examining the calculated trajectories as shown in Figure 22d. Oscillations of D and X are masked by intense fluctuations when the negative feedback is lost with $\alpha_1 = 0$ in Figure 22d, but the oscillations remain distinct when the negative feedback is strong enough with $\alpha_1 = 3$. The oscillation features with $\alpha_1 = 3$ are similar to those found in Figure 21a, which were calculated with $\alpha_1 = 1$. The weakening of oscillation for the small α_1 explains the behavior of δD in Figure 22a. As shown in Figure 22b, δD slightly decreases with small α_2. Trajectories in Figure 22e show that the oscillations of D and X become somewhat noisy when the positive feedback is lost with $\alpha_2 = 0$, while the oscillations turn into trains of pulses when the positive feedback is strong with $\alpha_2 = 3$. δD shows a peak at $\alpha_3 \approx 0.5$ and diminishes both at small and large α_3 as shown in Figure 22c. As shown in Figure 22f, the system tends to stay long at the small X and small D state with $\alpha_3 = 0$, which prevents oscillations. However, the system tends to stay at large D with the frequent noisy oscillation of X with large $\alpha_3 = 3$. Therefore, a suitable range of the coupling strength between ATPase reactions and structure is needed to keep the oscillation amplitude large.

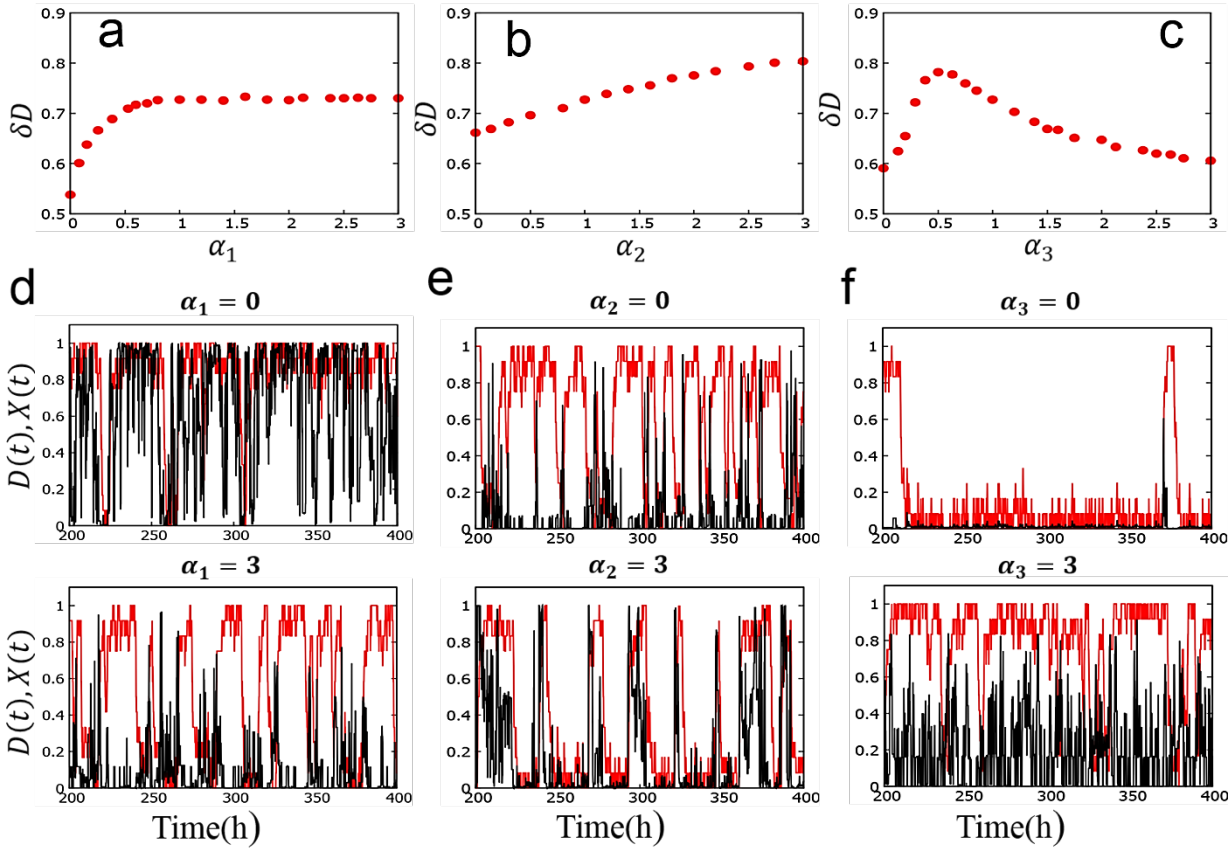

Figure 22: Effects of variation of the coupling strength between reactions and structure in the SM model. **a**) Oscillation amplitude δD is plotted as a function of the scaling factor α_1 of coupling between phosphorylation/dephosphorylation reactions at Ser431 and structure. $\alpha_2 = \alpha_3 = 1$. **b**) δD as a function of the scaling factor α_2 of coupling between phosphorylation/dephosphorylation reactions at Thr432 or Kai protein binding reactions and structure. $\alpha_1 = \alpha_3 = 1$. **c**) δD as a function of the scaling factor α_3 of coupling between ATPase reactions and structure. $\alpha_1 = \alpha_2 = 1$. Example trajectories of D (red) and X (black) calculated with **d**) $\alpha_1 = 0$ (upper panel) and $\alpha_1 = 3$ (lower panel) with $\alpha_2 = \alpha_3 = 1$, **e**) $\alpha_2 = 0$ (upper panel) and $\alpha_2 = 3$ (lower panel) with $\alpha_1 = \alpha_3 = 1$, and **f**) $\alpha_3 = 0$ (upper panel) and $\alpha_3 = 3$ (lower panel) with $\alpha_1 = \alpha_2 = 1$.

Variation of α_3 in the SM model correspond to the variation of q_0 in the MM model. In Figure 14 and Figure 15a, we find too small q_0 and too large q_0 prevent the system from oscillation. Thus, there is suitable range of perturbation on structure to generate a stable oscillation. As shown in Figure 21c, the system does not show oscillation when α_3 is too large or too small. Thus, the results of Figure.14, Figure. 15a and Figure. 22c suggest that the limited range of the perturbation of ATPase reactions on the structure is necessary both for single-molecule and ensemble-level oscillations. Although the overall trends of the effects of the perturbation of ATPase reactions in the MM (Figure 15a) and SM (Figure 22c) models are similar to each other, a dip of the oscillation amplitude as found in the MM model (Figure 15a) is absent from the SM model (Figure 22c). This absence of a dip should be because the subtle difference in oscillation modes, which was the reason to give a dip in the MM model, is varied and masked in the noisy stochastic behavior of the SM model.

To summarize the results, we find that the large amplitude oscillation in individual KaiC hexamers is supported by negative and positive feedback interactions in structure change as well as the suitable strength of coupling between ATPase reactions and structure change.

3.3.3 Correlation between ATPase activity and the oscillation frequency

The observed correlation between the frequency of ATP hydrolysis, or the ATPase activity, and the frequency of KaiC oscillation (Abe et al., 2015; Terauchi et al., 2007) is important for investigating the relationship between the ATPase reactions occurring in individual KaiC hexamer and the ensemble-level phosphorylation/dephosphorylation rhythm. As discussed in previous subsections, many features of the ensemble-level oscillation are already found in the single-

molecular level. Therefore, it is essential to analyze the relationship between the ATPase activity and the frequency of the single-molecular oscillation.

In Figure 23a, the single-molecular ATPase activity calculated with the SM model by introducing a scaling factor ε is shown. The rate constants of ATPase reactions defined in Eq. 29 were uniformly changed from the values of Table 2 as $k_{01}^{a,i} \rightarrow \varepsilon k_{01}^{a,i}$, $k_{10}^{a,i} \rightarrow \varepsilon k_{10}^{a,i}$, $k_{12}^{a,i} \rightarrow \varepsilon k_{12}^{a,i}$, $k_{21}^{a,i} \rightarrow \varepsilon k_{21}^{a,i}$, $k_{23}^{a,i} \rightarrow \varepsilon k_{23}^{a,i}$, and $k_{30}^{a,i} \rightarrow \varepsilon k_{30}^{a,i}$ with i = 1 and 0. For these scaled parameters with various values of ε, the number of released ADP molecules (i.e., the number of $a_i = 3 \rightarrow 0$ transitions) was counted as a measure of the ATPase activity in the absence of KaiA and KaiB, which was represented in the model by imposing $h_a^1 = h_b^0 = 0$. Also shown in Figure 23a is the averaged peak frequency of the power spectrum of the Fourier transform of the D oscillation calculated with nonzero h_a^1 and h_b^0 defined in Table 2 for the corresponding values of ε. Because of intense stochasticity in oscillations, the averaged peak frequency and its error bar were derived from extensive calculations. 50 power spectra were calculated from the Fourier transform of 50 trajectories of $D(t)$, with each trajectory having 2^{18} data points with regular steps mapped from calculated 2^{18} reaction steps as explained in Figure 20. Then, the peak of the spectrum obtained by averaging 50 spectra was identified. This calculation was repeated 100 times with different random numbers, and from the distribution of 100 peak frequencies, the averaged peak frequency was obtained and the error bars were calculated from the standard deviation. In spite of the intense stochasticity as seen from the large error bars in Figure 23a, we can see that the ATPase activity is correlated to the phosphorylation/dephosphorylation oscillation frequency in single KaiC hexamer.

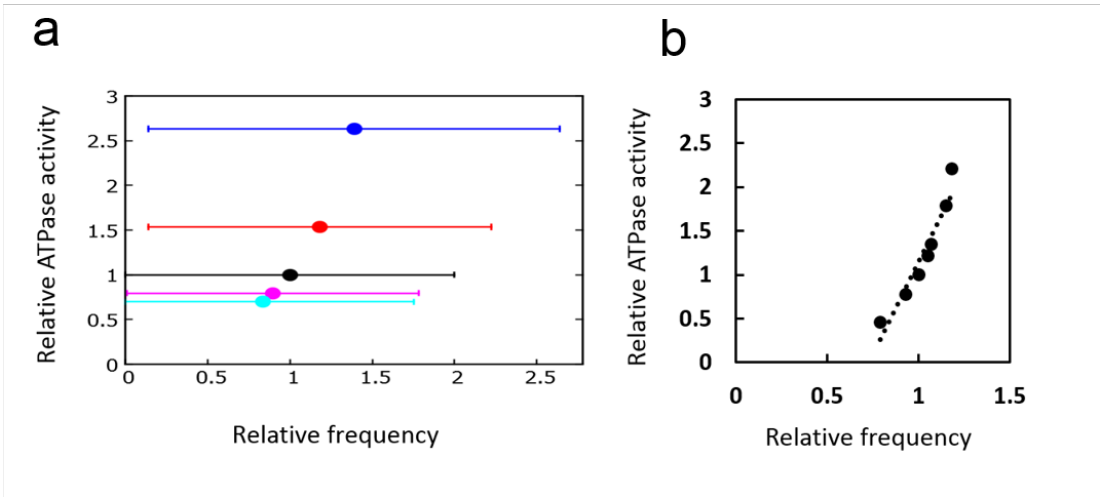

Figure 23: Correlation between ATPase activity and frequency of phosphorylation oscillation. **a**) Single-molecular correlation calculated with the SM model. Each point represents the ATPase activity calculated in the non-oscillatory condition and the average frequency calculated in the oscillatory condition for various scaling values ε of the ATPase reaction rates: ε = 4 (blue), ε = 2 (red), ε = 1 (black), ε = 0.6 (magenta), and ε = 0.4 (cyan). Error bars are the standard deviation of the distribution of the peak frequency of the Fourier transform spectra. The *p*-values calculated with the Mann-Whitney U test are $< 10^{-7}$ between distributions at ε = 0.4 (cyan) and ε = 4 (blue), 0.080 between ε = 0.4 (cyan) and ε = 1 (black), and 0.00087 between ε = 1 (black) and ε = 4 (blue). **b**) Ensemble-level correlation calculated with the MM model. Each point represents the ATPase activity calculated in the non-oscillatory condition and the average frequency calculated in the oscillatory condition for various values of f_0. Each point is the average of 10 trajectories, each of which is 2×10^3 h long. The panel **b** is the same graph as shown in Figure 15d but is replotted here by using the axes having the same scale as in **a**.

In Figure 23b, the results of the ensemble calculation with the MM model are plotted. Here, the number of released ADP in the ensemble were calculated in the condition of $A_T = B_T = 0$ with

various values of ATP hydrolysis frequency f_0, and the corresponding ensemble-level phosphorylation/dephosphorylation rhythm was calculated with the nonzero values of A_T and B_T as defined in Table 1. A distinct correlation between ATPase activity and the phosphorylation/dephosphorylation rhythm in the ensemble is shown in Figure 23b. Comparing the results of Figures 23a and 23b, we find that the important feature of the ensemble-level correlation between the ATPase activity and the phosphorylation/dephosphorylation rhythm already appears at the single-molecule level.

3.4 Summary of the analyses with the SM model

We developed a theoretical model of stochastic molecular processes of a single KaiC molecule. The oscillation dynamics of individual molecules were analyzed with this model in more detail than in the MM model. Because there has been no theoretical report to focus on the single-molecular behavior, the present analyses were the first attempt to do this. Simulation results with this SM model exhibited many features of the ensemble-level oscillation though the single-molecular oscillation carries intense stochastic fluctuation. Thus, the comparison between the SM and MM models suggests that the oscillation in individual molecules is the origin of the ensemble-level oscillation. Important results of the SM model are on the roles of ATPase reactions in the oscillation in a molecular level: Results of the SM model showed that the coupling between ATPase reactions and structure should be within a suitable range to maintain the large amplitude single-molecular oscillation. The correlation between ATPase activity and phosphorylation/dephosphorylation oscillation frequency at the single-molecule level was observed by this SM model. This result indicated that ATP hydrolysis reactions occurring stochastically in individual molecules should be the origin of the essential features of the

ensemble-level oscillation. Furthermore, the SM model provided information that was not available with the MM model: We found that the hexamer-level oscillation is wiped out when the cooperative structural interactions among subunits are lost. Among the four possible signs of b_1^{Thr} and b_1^{Ser} in Eq. 19, one particular choice of $(-+)$ explained the observed phase difference of phosphorylation oscillation at Thr432 and Ser431, which determined the balance between the negative feedback and positive feedback effects in KaiC hexamer.

Chapter 4: Conclusion

We described two coarse-grained theoretical models, the many-molecule (MM) model and the single-molecule (SM) model, to obtain a unified view of microscopic and macroscopic processes of the cyanobacterial clockwork. These two theoretical models described the mechanism how the microscopic structure and chemical reactions influence the circadian oscillation. In particular, these models suggested that the role of ATP hydrolysis both in a large number of KaiC molecules and in individual KaiC molecules is a key for understanding the relations between microscopic and macroscopic processes.

To analyze the relation between microscopic and macroscopic processes, we need to investigate both of two problems, the problem of coherence in oscillation of individual molecules, and the problem of synchronization of many molecules. In the SM model, we examined how the coherence in oscillations of individual KaiC molecules is brought about in spite of the noisy intra-molecular fluctuations, whereas in the MM model, the intra-molecular dynamics were described in a simplified way and we focused on synchronization among many KaiC molecules. Detailed computational analysis of these models suggested that the oscillation frequency of individual KaiC molecule is correlated to the ATPase activity within individual KaiC molecules. Moreover, the ATP hydrolysis in individual KaiC molecules was found to be essential for temperature compensation and to maintain the synchronization of many KaiC molecules. Therefore, we concluded that the ATPase activity of individual KaiC molecules is a determining feature of the ensemble-level oscillation of this unique clock machinery.

Here, we briefly summarize the importance of researches on the cyanobacterial circadian clock and then summarize the assumptions used in developing the models. For a long time in the past, it was widely believed that prokaryotes are too simple and have a too short life cycle to have

evolved circadian programs. However, the cyanobacterial circadian system has emerged from a scientific curiosity to a major model system for analyzing clock phenomena. The cyanobacterial circadian system is the only clock system in which all the essential proteins of the core oscillator, KaiA, KaiB and KaiC, have been crystallized and structurally determined (Ye et al., 2004; Hitomi et al., 2005; Pattanayek et al., 2004). A biochemical oscillator was reconstituted *in vitro* with these three purified Kai proteins and ATP, which displays the key properties of temperature-compensated rhythmicity (Nakajima et al., 2005). The rhythmic association of KaiA and KaiB with KaiC is essential for the generation of robust phosphorylation rhythm (Kageyama et al., 2006). KaiC consists of two highly homologous domains, called the CI and CII domains (Mori et al., 2002). Both domains can bind and hydrolyze ATP but only the CII domain can be phosphorylated with two phosphorylation sites per monomer, Ser431 and Thr432 (Nishiwaki et al., 2004). The ATPase activity of KaiC, which is extremely low and is kept constant in a range of physiological temperatures, plays a central role in generating the temperature compensated circadian period of the Kai oscillator. The ATP regeneration experiments indicated that the phosphorylation and dephosphorylation of the CII domain proceed via the transfer of phosphate groups between the threonine/serine residues and the nucleotide bound to the CII domain (Egli et al., 2012; Nishiwaki & Kondo, 2012). Therefore, we can guess that with the efficiency of about 50%, the ATP hydrolysis in the CII domain is used for the phosphorylation. It is rather obvious that the frequency of this ATP hydrolysis in the CII domain is correlated to the frequency of the oscillation of the phosphorylation level. However, about 10 ATP molecules are hydrolyzed in the CI domain, and the frequency of this ATP hydrolysis measured in the non-oscillatory condition is correlated to the oscillation frequency of the phosphorylation level in the CII domain in the oscillatory condition (Abe et al., 2015). While it is clear that the clock is driven by the turnover of

ATP (Murakami et al., 2008; Terauchi et al., 2007), how ATP hydrolysis in the CI domain drives the phosphorylation oscillation was still unclear. Therefore, a theoretical study is necessary for clarifying the mechanism, and our proposed two models were the first attempt to resolve this problem. In the two theoretical models described in this dissertation, we assumed that KaiC hexamers undergo an allosteric transition between the tight and loose two conformational states. The binding affinity of KaiA and KaiB to KaiC depends on the conformational states of KaiC hexamer and whether KaiA is bound or not, affects the rate of phosphorylation/dephosphorylation reactions. This assumption should be reasonable because the atomic positions of the phosphorylation site, Ser431 and Thr432, are distant from the binding sites of KaiA (Pattanayek et al., 2006) and KaiB (Snijder et al., 2017). Thus, the allosteric communication through the structural change should mediate the effects of phosphorylation/dephosphorylation reactions and binding of KaiA or KaiB. The ATP hydrolysis in the CI domain and phosphorylation in the CII domain are coupled through the allosteric communication, which facilitates the effects of ATP reactions on the phosphorylation/dephosphorylation reactions. Hence, we assume that the ATPase activity in the CI domain brings perturbation on allosteric transitions of the KaiC hexamer and controls the binding affinity of KaiA and KaiB. This assumption is consistent with the recently published fluorescence spectroscopic study, which reported that the CI ring undergoes a structural transition, which is driven by the ATP hydrolysis in the CI domain, and that this transition is necessary for the binding of KaiB to KaiC (Mukaiyama et al., 2018).

The analyses with the result of the MM model suggested that the synchronization of individual stochastic oscillations is maintained by the sequestration of KaiA into the KaiABC complex and ATP hydrolysis helps individual molecules to enhance the effects of this sequestration. ATP hydrolysis reactions randomly occurring in the CI domain induce the frequent

structural modulation and perturb each KaiC hexamer to generate the ensemble-level oscillation. Thus, both KaiA sequestration and ATP hydrolysis are necessary to give rise to a coherent oscillation. The correlation between ATPase activity and the frequency of phosphorylation oscillation was also observed with the MM model, which was consistent with the experiment (Abe et al., 2015, Terauchi et al., 2007). Temperature dependence of period and amplitude of the ensemble oscillation were analyzed by using the MM model. We assumed that the lifetime of the ADP-bound state in the CI domain should become small with increased temperature, and this assumption can explain the temperature compensation of the oscillation period. A possible molecular mechanism of the strong temperature dependence of the lifetime of the ADP bound state is the large activation energy of molecular gating that opens/closes a pathway for the ADP to be released from the KaiC. This hypothesis could be checked experimentally by comparing mutants having substituted amino acid residues near the ADP ejection pathway, which should change the lifetime of the ADP bound state. The too long lifetime of ADP bound state at low temperature brings disappearance of oscillation, which is consistent with the experimental observation (Murayama et al., 2017).

The simulated oscillation results of the SM model showed that many features of the ensemble-level oscillation exist already in the oscillation of single KaiC molecule. In the SM model, we found that a suitable range of perturbation of ATPase reactions on the structure is needed to keep the amplitude of the single-molecular oscillation large. The ATPase activity is correlated to the frequency of the phosphorylation oscillation at the single-molecule level, which should be the origin of the observed correlation between the ATPase activity and oscillation frequency in the ensemble level. Thus, the perturbation on the structure by the ATPase reactions in individual molecules is a key determinant of the oscillation frequency and amplitude in the

ensemble of many molecules. Furthermore, the SM model revealed that the noisy fluctuations of individual subunits are suppressed by the cooperative structural interactions among subunits, which gives rise to the coherent oscillation in the single-molecular level. This cooperative mechanism should be further examined by the mutational and structural experimental studies. The SM model was suited to examine the relation and the relative balance among negative and positive feedback interactions, and the model revealed that such a balance is essential for explaining the phase difference of oscillations at Thr432 and Ser431.

Computational studies of both the proposed MM and SM models suggested that ATP hydrolysis reactions that are stochastically occurring in the CI domains of individual KaiC hexamers play significant roles in synchronization, temperature compensation, and frequency determination at the ensemble-level oscillation. It is possible to consider the model of many KaiC hexamers by retaining the high-resolution description of each hexamer as in the SM model. This is a possible extension of the present study. Because a large number of reactions are considered in such a model, the efficient algorithm should be necessary for simulating the stochastic dynamics of many KaiC hexamers with that resolution. By using such modelling, it should be interesting to see whether the temperature compensation is realized in the single-molecular level. To further validate the hypotheses proposed in this study, the present 'mesoscopic' models should be compared with the microscopic atomic-level observations of structure and reactions (Abe et al., 2015) and also with the macroscopic ensemble-level observations of phase shift, synchronization, and entrainment (Ito et al., 2007; Yoshida et al., 2009). In this way, a much broader and comprehensive picture that unifies explanations of microscopic through macroscopic phenomena should open a new perspective of biomolecular systems that are working coherently in the living cellular organism of the cyanobacteria.

References

Abe, J., Hiyama, T.B., Mukaiyama, A., Son, S., Mori, T., Saito, S., Osako, M., Wolanin, J., Yamashita, E., Kondo, T. and Akiyama, S. (2015). Atomic-scale origins of slowness in the cyanobacterial circadian clock. *Science,* **349**, 312-316. doi:10.1126/science.1261040

Akiyama, S., Nohara, A., Ito, K., & Maéda, Y. (2008). Assembly and Disassembly Dynamics of the Cyanobacterial Periodosome. *Molecular Cell,* **29**, 703-716. doi:10.1016/j.molcel.2008.01.015

Aschoff, J. (1967). Human circadian rhythms in activity, body temperature and other functions. *Life Sci Space Res,* **5**, 159-173.

Aschoff, J. (1969). Desynchronization and resynchronization of human circadian rhythms. *Aerosp Med,* **40**, 844-849.

Aschoff, J., & Wever, R. (1976). Human circadian rhythms: a multioscillatory system. *Fed Proc,* **35**, 236-232.

Brettschneider, C., Rose, R.J., Hertel, S., Axmann, I.M., Heck, A.J. and Kollmann, M. (2010). A sequestration feedback determines dynamics and temperature entrainment of the KaiABC circadian clock. *Molecular Systems Biology*, **6**, 389-389

Chang, Y.G., Cohen, S.E., Phong, C., Myers, W.K., Kim, Y.I., Tseng, R., Lin, J., Zhang, L., Boyd, J.S., Lee, Y. and Kang, S. (2015). A protein fold switch joins the circadian oscillator to clock output in cyanobacteria. *Science*, **349**, 324-328. doi:10.1126/science.1260031

Chang, Y.-G., Kuo, N.-W., Tseng, R., & LiWang, A. (2011). Flexibility of the C-terminal, or CII, ring of KaiC governs the rhythm of the circadian clock of cyanobacteria. *Proceedings of the National Academy of Sciences USA,* **108**, 14431-14436. doi:10.1073/pnas.1104221108

Chang, Y.-G., Tseng, R., Kuo, N.-W., & LiWang, A. (2012). Rhythmic ring–ring stacking drives the circadian oscillator clockwise. *Proceedings of the National Academy of Sciences USA,* **109**, 16847-16851. doi:10.1073/pnas.1211508109

Das, S., Terada, T. P., & Sasai, M. (2017). Role of ATP Hydrolysis in Cyanobacterial Circadian Oscillator. *Scientific Reports,* **7**, 17469. doi:10.1038/s41598-017-17717-z

DeCoursey, P. J., Dunlap, J. C., & Loros, J. J. (2004). *Chronobiology: biological timekeeping*. Sunderland, MA, US: Sinauer Associates.

de Mairan, J. D. (1729). Observation botanique. *Histoire de l'Académie Royale des Sciences Paris*.

Dunlap, J.C. (1999). Molecular bases for circadian clocks. *Cell*, **96**, 271-290.

Egli, M., Mori, T., Pattanayek, R., Xu, Y., Qin, X., & Johnson, C. H. (2012). Dephosphorylation of the Core Clock Protein KaiC in the Cyanobacterial KaiABC Circadian Oscillator Proceeds via an ATP Synthase Mechanism. *Biochemistry,* **51**, 1547-1558. doi:10.1021/bi201525n

Eguchi, K., Yoda, M., Terada, T. P., & Sasai, M. (2008). Mechanism of robust circadian oscillation of KaiC phosphorylation in vitro. *Biophysical Journal,* **95**, 1773-1784. doi: 10.1529/biophysj.107.127555

Garces, R. G., Wu, N., Gillon, W., & Pai, E. F. (2004). Anabaena circadian clock proteins KaiA and KaiB reveal a potential common binding site to their partner KaiC. *The EMBO Journal,* **23**, 1688-1698. doi: 10.1038/sj.emboj.7600190

Gillespie, D. T. (1977). Exact stochastic simulation of coupled chemical reactions. *The Journal of Physical Chemistry,* **81**, 2340-2361.

Grobbelaar, N., Huang, T.C., Lin, H.Y. and Chow, T.J. (1986). Dinitrogen-fixing endogenous rhythm in Synechococcus RF-1. *FEMS Microbiology Letters,* **37**, 173-177. doi:10.1111/j.1574-6968.1986.tb01788.x

Halberg, F., Carandente, F., Cornelissen, G., & Katinas, G. S. (1977). Glossary of chronobiology (author's transl). *Chronobiologia,* **4** Suppl 1, 1-189.

Hatakeyama, T. S., & Kaneko, K. (2012). Generic temperature compensation of biological clocks by autonomous regulation of catalyst concentration. *Proceedings of the National Academy of Sciences USA,* **109**, 8109-8114. doi:10.1073/pnas.1120711109

Hitomi, K., Oyama, T., Han, S., Arvai, A. S., & Getzoff, E. D. (2005). Tetrameric architecture of the circadian clock protein KaiB a novel interface for intermolecular interactions and its impact on the circadian rhythm. *Journal of Biological Chemistry,* **280**, 19127-19135.

Huang, T.-C., & Grobbelaar, N. (1995). The circadian clock in the prokaryote Synechococcus RF-1. *Microbiology,* **141**, 535-540.

Ishiura, M., Kutsuna, S., Aoki, S., Iwasaki, H., Andersson, C.R., Tanabe, A., Golden, S.S., Johnson, C.H. and Kondo, T. (1998). Expression of a gene cluster kaiABC as a circadian feedback process in cyanobacteria. *Science,* **281**, 1519-1523. doi: 10.1126/science.281.5382.1519

Iwasaki, H., Nishiwaki, T., Kitayama, Y., Nakajima, M., & Kondo, T. (2002). KaiA-stimulated KaiC phosphorylation in circadian timing loops in cyanobacteria. *Proceedings of the National Academy of Sciences USA,* **99**, 15788-15793. doi:10.1073/pnas.222467299

Iwasaki, H., Taniguchi, Y., Ishiura, M., & Kondo, T. (1999). Physical interactions among circadian clock proteins KaiA, KaiB and KaiC in cyanobacteria. *The EMBO Journal,* **18**, 1137-1145. doi:10.1093/emboj/18.5.1137

Iwase, R., Imada, K., Hayashi, F., Uzumaki, T., Morishita, M., Onai, K., Furukawa, Y., Namba, K. and Ishiura, M. (2005). Functionally important substructures of circadian clock protein KaiB in a unique tetramer complex. *Journal of Biological Chemistry,* **280**, 43141-43149. doi: 10.1074/jbc.M503360200

Kageyama, H., Kondo, T., & Iwasaki, H. (2003). Circadian formation of clock protein complexes by KaiA, KaiB, KaiC, and SasA in cyanobacteria. *Journal of Biological Chemistry,* **278**, 2388-2395. doi: 10.1074/jbc.M208899200

Kageyama, H., Nishiwaki, T., Nakajima, M., Iwasaki, H., Oyama, T., & Kondo, T. (2006). Cyanobacterial Circadian Pacemaker: Kai Protein Complex Dynamics in the KaiC Phosphorylation Cycle In Vitro. *Molecular Cell,* **23**, 161-171. doi: 10.1016/j.molcel.2006.05.039

Kim, Y.-I., Dong, G., Carruthers, C. W., Golden, S. S., & LiWang, A. (2008). The day/night switch in KaiC, a central oscillator component of the circadian clock of cyanobacteria. *Proceedings of the National Academy of Sciences USA,* **105**, 12825-12830. doi:10.1073/pnas.0800526105

Kitayama, Y., Iwasaki, H., Nishiwaki, T., & Kondo, T. (2003). KaiB functions as an attenuator of KaiC phosphorylation in the cyanobacterial circadian clock system. *The EMBO Journal,* **22**, 2127-2134. doi:10.1093/emboj/cdg212

Kondo, T., Strayer, C. A., Kulkarni, R. D., Taylor, W., Ishiura, M., Golden, S. S., & Johnson, C. H. (1993). Circadian rhythms in prokaryotes: luciferase as a reporter of circadian gene expression in cyanobacteria. *Proceedings of the National Academy of Sciences USA,* **90**, 5672-5676. doi:10.1073/pnas.90.12.5672

Konopka, R. J., & Benzer, S. (1971). Clock mutants of Drosophila melanogaster. *Proceedings of the National Academy of Sciences USA,* **68**, 2112-2116.

Mitsui, A., Kumazawa, S., Takahashi, A., Ikemoto, H., Cao, S., & Arai, T. (1986). Strategy by which nitrogen-fixing unicellular cyanobacteria grow photoautotrophically. *Nature,* **323**, 720-722. doi:10.1038/323720a0

Mori, T., Saveliev, S. V., Xu, Y., Stafford, W. F., Cox, M. M., Inman, R. B., & Johnson, C. H. (2002). Circadian clock protein KaiC forms ATP-dependent hexameric rings and binds DNA. *Proceedings of the National Academy of Sciences USA,* **99**, 17203-17208. doi:10.1073/pnas.262578499

Mori, T., Williams, D.R., Byrne, M.O., Qin, X., Egli, M., Mchaourab, H.S., Stewart, P.L. and Johnson, C.H. (2007). Elucidating the ticking of an in vitro circadian clockwork. *PLoS Biology*, **5**, e93.

Mukaiyama, A., Furuike, Y., Abe, J., Yamashita, E., Kondo, T., & Akiyama, S. (2018). Conformational rearrangements of the C1 ring in KaiC measure the timing of assembly with KaiB. *Scientific Reports,* **8**, 8803. doi:10.1038/s41598-018-27131-8

Murakami, R., Miyake, A., Iwase, R., Hayashi, F., Uzumaki, T., & Ishiura, M. (2008). ATPase activity and its temperature compensation of the cyanobacterial clock protein KaiC. *Genes to Cells,* **13**, 387-395. doi:10.1111/j.1365-2443.2008.01174.x

Murayama, Y., Kori, H., Oshima, C., Kondo, T., Iwasaki, H., & Ito, H. (2017). Low temperature nullifies the circadian clock in cyanobacteria through Hopf bifurcation. *Proceedings of the National Academy of Sciences USA,* **114**, 5641-5646. doi:10.1073/pnas.1620378114

Murayama, Y., Mukaiyama, A., Imai, K., Onoue, Y., Tsunoda, A., Nohara, A., Ishida, T., Maéda, Y., Terauchi, K., Kondo, T. and Akiyama, S. (2011). Tracking and visualizing the circadian ticking of the cyanobacterial clock protein KaiC in solution. *The EMBO journal*, **30**, 68-78.

Mutoh, R., Nishimura, A., Yasui, S., Onai, K., & Ishiura, M. (2013). The ATP-Mediated Regulation of KaiB-KaiC Interaction in the Cyanobacterial Circadian Clock. *PLoS One,* **8**, e80200. doi:10.1371/journal.pone.0080200

Nagai, T., Terada, T. P., & Sasai, M. (2010). Synchronization of circadian oscillation of phosphorylation level of KaiC in vitro. *Biophysical Journal,* **98**, 2469-2477. doi:10.1016/j.bpj.2010.02.036

Nakajima, M., Imai, K., Ito, H., Nishiwaki, T., Murayama, Y., Iwasaki, H., Oyama, T. and Kondo, T. (2005). Reconstitution of circadian oscillation of cyanobacterial KaiC phosphorylation in vitro. *Science*, **308**, 414-415.

Nakajima, M., Ito, H. and Kondo, T. (2010). In vitro regulation of circadian phosphorylation rhythm of cyanobacterial clock protein KaiC by KaiA and KaiB. *FEBS Letters*, **584**, 898-902. doi:10.1016/j.febslet.2010.01.016

Nishiwaki, T., & Kondo, T. (2012). Circadian autodephosphorylation of cyanobacterial clock protein KaiC occurs via formation of ATP as intermediate. *Journal of Biological Chemistry,* **287**, 18030-18035.

Nishiwaki, T., Satomi, Y., Kitayama, Y., Terauchi, K., Kiyohara, R., Takao, T., & Kondo, T. (2007). A sequential program of dual phosphorylation of KaiC as a basis for circadian rhythm in cyanobacteria. *The EMBO Journal,* **26**, 4029-4037. doi:10.1038/sj.emboj.7601832

Nishiwaki, T., Satomi, Y., Nakajima, M., Lee, C., Kiyohara, R., Kageyama, H., Kitayama, Y., Temamoto, M., Yamaguchi, A., Hijikata, A. and Go, M. (2004). Role of KaiC phosphorylation in the circadian clock system of Synechococcus elongatus PCC 7942. *Proceedings of the National Academy of Sciences USA,* **101**, 13927-13932.

Northrup, S. H., & Erickson, H. P. (1992). Kinetics of protein-protein association explained by Brownian dynamics computer simulation. *Proceedings of the National Academy of Sciences USA*, **89**, 3338-3342.

Oyama, K., Azai, C., Nakamura, K., Tanaka, S., & Terauchi, K. (2016). Conversion between two conformational states of KaiC is induced by ATP hydrolysis as a trigger for cyanobacterial circadian oscillation. *Scientific Reports,* **6**, 32443. doi:10.1038/srep32443

Paijmans, J., Lubensky, D. K., & ten Wolde, P. R. (2017). A thermodynamically consistent model of the post-translational Kai circadian clock. *PLoS Computational Biology,* **13**, e1005415. doi:10.1371/journal.pcbi.1005415

Pattanayek, R., Wang, J., Mori, T., Xu, Y., Johnson, C. H., & Egli, M. (2004). Visualizing a Circadian Clock Protein: Crystal Structure of KaiC and Functional Insights. *Molecular Cell,* **15**, 375-388. doi:10.1016/j.molcel.2004.07.013

Pattanayek, R., Williams, D. R., Pattanayek, S., Xu, Y., Mori, T., Johnson, C. H., Stewart, P.L. and Egli, M. (2006). Analysis of KaiA–KaiC protein interactions in the cyano-bacterial circadian clock using hybrid structural methods. *The EMBO Journal,* **25**, 2017-2028. doi:10.1038/sj.emboj.7601086

Phong, C., Markson, J. S., Wilhoite, C. M., & Rust, M. J. (2013). Robust and tunable circadian rhythms from differentially sensitive catalytic domains. *Proceedings of the National Academy of Sciences USA,* **110**, 1124-1129. doi:10.1073/pnas.1212113110

Rust, M. J., Markson, J. S., Lane, W. S., Fisher, D. S., & O'Shea, E. K. (2007). Ordered phosphorylation governs oscillation of a three-protein circadian clock. *Science,* **318**, 809-812. doi:10.1126/science.1148596

Snijder, J., Burnley, R. J., Wiegard, A., Melquiond, A. S. J., Bonvin, A. M. J. J., Axmann, I. M., & Heck, A. J. R. (2014). Insight into cyanobacterial circadian timing from structural details of the KaiB–KaiC interaction. *Proceedings of the National Academy of Sciences USA,* **111**, 1379-1384. doi:10.1073/pnas.1314326111

Snijder, J., Schuller, J. M., Wiegard, A., Lössl, P., Schmelling, N., Axmann, I. M., Plitzko, J.M., Förster, F. and Heck, A. J. R. (2017). Structures of the cyanobacterial circadian oscillator frozen in a fully assembled state. *Science,* **355**, 1181-1184. doi:10.1126/science.aag3218

Sompolinsky, H. and Zippelius, A. (1982). Relaxational dynamics of the Edwards-Anderson model and the mean-field theory of spin-glasses. *Physical Review B*, **25**, 6860 -6875.

Stal, L. J., & Krumbein, W. E. (1985). Nitrogenase activity in the non-heterocystous cyanobacterium Oscillatoria sp. grown under alternating light-dark cycles. *Archives of Microbiology,* **143**, 67-71. doi:10.1007/bf00414770

Takigawa-Imamura, H., & Mochizuki, A. (2006). Predicting Regulation of the Phosphorylation Cycle of KaiC Clock Protein Using Mathematical Analysis. *Journal of Biological Rhythms,* **21**, 405-416. doi:10.1177/0748730406291329

Terauchi, K., Kitayama, Y., Nishiwaki, T., Miwa, K., Murayama, Y., Oyama, T., & Kondo, T. (2007). ATPase activity of KaiC determines the basic timing for circadian clock of cyanobacteria. *Proceedings of the National Academy of Sciences USA,* **104**, 16377-16381. doi:10.1073/pnas.0706292104

Tomita, J., Nakajima, M., Kondo, T., & Iwasaki, H. (2005). No transcription-translation feedback in circadian rhythm of KaiC phosphorylation. *Science,* **307**, 251-254. doi:10.1126/science.1102540

Uzumaki, T., Fujita, M., Nakatsu, T., Hayashi, F., Shibata, H., Itoh, N., Kato, H. and Ishiura, M. (2004). Crystal structure of the C-terminal clock-oscillator domain of the cyanobacterial KaiA protein. *Nature Structural & Molecular Biology,* **11**, 623. doi:10.1038/nsmb781

Vakonakis, I., & LiWang, A. C. (2004). Structure of the C-terminal domain of the clock protein KaiA in complex with a KaiC-derived peptide: Implications for KaiC regulation. *Proceedings of the National Academy of Sciences USA,* **101**, 10925-10930. doi:10.1073/pnas.0403037101

Vakonakis, I., Sun, J., Wu, T., Holzenburg, A., Golden, S. S., & LiWang, A. C. (2004). NMR structure of the KaiC-interacting C-terminal domain of KaiA, a circadian clock protein: Implications for KaiA–KaiC interaction. *Proceedings of the National Academy of Sciences USA,* **101**, 1479-1484. doi:10.1073/pnas.0305516101

van Zon, J. S., Lubensky, D. K., Altena, P. R. H., & ten Wolde, P. R. (2007). An allosteric model of circadian KaiC phosphorylation. *Proceedings of the National Academy of Sciences USA,* **104**, 7420-7425. doi:10.1073/pnas.0608665104

Wang, J., Xu, L., & Wang, E. (2009). Robustness and coherence of a three-protein circadian oscillator: landscape and flux perspectives. *Biophysical Journal,* **97**, 3038-3046. doi:10.1016/j.bpj.2009.09.021

Wood, T. L., Bridwell-Rabb, J., Kim, Y.-I., Gao, T., Chang, Y.-G., LiWang, A., Barondeau, D.P. and Golden, S. S. (2010). The KaiA protein of the cyanobacterial circadian oscillator is modulated by a redox-active cofactor. *Proceedings of the National Academy of Sciences USA,* **107**, 5804-5809. doi:10.1073/pnas.0910141107

Xu, Y., Mori, T., & Johnson, C. H. (2003a). Cyanobacterial circadian clockwork: roles of KaiA, KaiB and the kaiBC promoter in regulating KaiC. *The EMBO Journal,* **22**, 2117-2126. doi:10.1093/emboj/cdg168

Xu, Y., Mori, T., Pattanayek, R., Pattanayek, S., Egli, M., & Johnson, C. H. (2004). Identification of key phosphorylation sites in the circadian clock protein KaiC by crystallographic and mutagenetic analyses. *Proceedings of the National Academy of Sciences USA,* **101**, 13933-13938. doi:10.1073/pnas.0404768101

Ye, S., Vakonakis, I., Ioerger, T. R., LiWang, A. C., & Sacchettini, J. C. (2004). Crystal structure of circadian clock protein KaiA from Synechococcus elongatus. *Journal of Biological Chemistry,* **279**, 20511-20518. doi: 10.1074/jbc.M400077200

Yoda, M., Eguchi, K., Terada, T. P., & Sasai, M. (2007). Monomer-shuffling and allosteric transition in KaiC circadian oscillation. *PLoS One,* **2**, e408. doi:10.1371/journal.pone.0000408

Yoshida, T., Murayama, Y., Ito, H., Kageyama, H., & Kondo, T. (2009). Nonparametric entrainment of the in vitro circadian phosphorylation rhythm of cyanobacterial KaiC by temperature cycle. *Proceedings of the National Academy of Sciences USA,* **106**, 1648-1653. doi:10.1073/pnas.0806741106

Acknowledgement

First and foremost, I would like to acknowledge my gratitude and gratefulness to my Ph.D. supervisor Professor Dr. Masaki Sasai for his instruction, mentoring, thoughtful suggestions and guidance throughout my doctoral course study. He guided me during the whole time of my doctoral research and also during the writing of this thesis. Dr. Sasai has not only been ideologically supportive, but also has given me enough freedom to put my thought in my work. His innovative ideas in solving the mystery of the circadian clockwork in cyanobacteria, and extensive knowledge in diverse field of sciences are an important part of the treasures that enormously helped me during my graduate study. This dissertation work would have not been done without the continuous support from him.

I am especially grateful to Dr. Tomoki P. Terada, who guides my research with his constructive suggestions and thoughtful discussions. I also show my acknowledgement to Dr. George Chikenji. He provided very important technical support that was very helpful for my study. I would especially like to thank Dr. S. S. Ashwin. He has taught me more than I could ever give him credit for here. I gratefully thank and show my gratitude to Dr. Bhaswati Bhattacharyya for her constant support during my study. More essentially, I acknowledge my gratitude to all current and alumni members of the Sasai lab. I also show my gratitude to the Otsuka Toshimi Scholarship Foundation of Japan for their financial support.

Nobody has been more important to me than the members of my family in the pursuit of this project. I would like to thank my parents; whose love and guidance are with me in whatever I pursue. Mostly, I wish to thank my husband, Srikanta Chowdhury, who provides unending inspiration and practical support during the whole period of my study.

List of publications and presentations for the present study

Publications:

- Sumita Das, Tomoki P. Terada, and Masaki Sasai (2017). Role of ATP Hydrolysis in Cyanobacterial Circadian Oscillator. *Scientific Reports*, **7**:17469. doi:10.1038/s41598-017-17717-z
- Sumita Das, Tomoki P. Terada, and Masaki Sasai (2018). Single-molecular and ensemble-level oscillations of cyanobacterial circadian clock. *Biophysics and Physicobiology,* **15**: 136-150. doi:10.2142/biophysico.15.0_136

Presentations:

- Poster: The 53rd Annual Meeting of the Biophysical Society of Japan, September 13-15, 2015, Kanazawa University, Japan. Sumita Das, Shota Hashimoto, Tomoki P. Terada, Masaki Sasai. A stochastic simulation study on circadian oscillation and ATPase activity of KaiC hexamer.
- Poster: The 54th Annual Meeting of the Biophysical Society of Japan, November 25-27, 2016, Tsukuba International Congress Center, Japan. Sumita Das, Shota Hashimoto, Tomoki P. Terada, Masaki Sasai. A stochastic simulation study on the correlation between circadian oscillation and ATPase activity of KaiC hexamer (*Awarded as the best student presentation award*).
- Poster: The 55th Annual Meeting of the Biophysical Society of Japan, September 19-21, 2017, Kumamoto University, Japan. Sumita Das, Shota Hashimoto, Tomoki P. Terada,

Masaki Sasai. Regulation of circadian oscillation by the ATPase activity of KaiC in Cyanobacteria.

- Poster: Cyanoclock1.0, June 29-30, 2018, Nagoya University, Japan. Sumita Das, Tomoki P. Terada, and Masaki Sasai. ATPase activity of individual KaiC molecules is a key determinant for the ensemble-level oscillation of cyanobacterial KaiABC system.